Nonlinear Ultrasonics: Signal Processing Considerations and a Nonlinear Parameter for Rayleigh Waves

A Thesis
Presented to
The Academic Faculty

by

Thorsten Mueller

In Partial Fulfillment
of the Requirements for the Degree
Master of Science in Engineering Science and Mechanics

School of Civil and Environmental Engineering
Georgia Institute of Technology
December 2005

Nonlinear Ultrasonics: Signal Processing Considerations and a Nonlinear Parameter for Rayleigh Waves

Approved by:

Dr. Laurence Jacobs, Committee Chair
School of Civil and Environmental Engineering
Georgia Institute of Technology

Dr. Jianmin Qu
George W. Woodruff School of Mechanical Engineering
Georgia Institute of Technology

Dr. Jin-Yeon Kim
George W. Woodruff School of Mechanical Engineering
Georgia Institute of Technology

Date Approved: September 9, 2005

ACKNOWLEDGEMENTS

I would like to express my gratitude to Prof. Laurence J. Jacobs for being an outstanding advisor as well as a good friend. He supported and motivated me throughout my thesis and my many discussions with him have helped me keep on the right track. As a friend he gave me advice not only for my thesis and was ambitious to help as much as possible whenever help was needed. I'm also very thankful for giving me the opportunity to present results of this thesis at the QNDE Conference 2005 in Brunswick, Maine.

I'm also deeply indebted to Dr. Jin-Yeon Kim without whom my thesis would not be as it is. With his extraordinary knowledge and experience in ultrasonics he gave me lots of ideas and was always open for fruitful discussions. I have enjoyed every discussion, not only about my thesis, with him.

My thank also goes to Prof. Jianmin Qu who gave me advise for the Rayleigh waves and is a member in my thesis committee.

Furthermore I would like to thank my colleagues and friends in the Lab, Jeff Davis, Ben Mason, Jan Herrmann, Helge Kuttig, Kritsakorn Luangvilai and Wonsiri Punurai for all the help I got, the great atmosphere in the Lab and the time we have spent together.

Although not directly involved in my work at Georgia Tech, my thanks go to Prof. Lothar Gaul for giving me the opportunity to study at Georgia Tech by choosing me as a candidate for this ISAP Program. My studies were made possible by the generous financial support of the DAAD (German Academic Exchange Service).

Having had the great opportunity to spend more than one year abroad, I want to express my deepest gratitude to my parents and my family for their generous and

loving support of my stay in the US. Many thanks go also to all my friends at home who have kept contact with me throughout this time. I'm thankful to all the new friends I have made here in the US, for their support, the great times we had and the unforgettable memories we share together.

TABLE OF CONTENTS

ACKNOWLEDGEMENTS . . . . . **iii**

LIST OF TABLES . . . . . **viii**

LIST OF FIGURES . . . . . **ix**

SUMMARY . . . . . **xii**

I INTRODUCTION **1**

II WAVE PROPAGATION IN SOLIDS **3**

2.1 Equations of Motion 3

2.2 Linear Wave Propagation 4

2.2.1 Linear Elasticity 4

2.2.2 Linear Wave Phenomena 6

2.3 Nonlinear Wave Propagation 7

2.3.1 Strain Energy and Third-order Elastic Constants 7

2.3.2 Nonlinear Wave Equation 8

2.4 Nonlinear Parameter β 8

2.4.1 Material Property Dependency of β 9

2.4.2 β in Terms of Harmonic Amplitudes 9

III NONLINEAR MEASUREMENTS **11**

3.1 Principle of Nonlinear Measurements 11

3.2 Measurement of the Nonlinear Parameter using Contact Transducers 12

3.3 Measurement of the Nonlinear Parameter using Laser Ultrasound . . 13

IV SIGNAL PROCESSING FOR NONLINEAR MEASUREMENTS 15

4.1 The Discrete Fourier Transform 15

4.1.1 Definition 15

4.1.2 Nyquist Sampling Theorem 16

4.1.3 Fast Fourier Transform (FFT) 17

4.1.4 Zero-Padding . . . 17
4.1.5 Properties of the DFT . . . 19
4.2 DFT of Harmonic Signals - Demonstration Example . . . 21
4.3 Windows for Harmonic Analysis . . . 22
4.3.1 Spectral Leakage . . . 23
4.3.2 Commonly used Windows . . . 24
4.3.3 Correction of the Amplitude for Windows . . . 26
4.3.4 The Rectangular Window . . . 28
4.3.5 How to Chose a Window . . . 29
4.3.6 Multiple Windows . . . 30
4.3.7 DC Part and Windowing . . . 31
4.3.8 Rules of Thumb . . . 31
4.4 Filtering for Harmonic Amplitudes . . . 32
4.5 Pulse Inversion . . . 33
4.6 Example . . . 34
4.7 Further Signal Processing Methods for Nonlinear Measurements . . 38
4.7.1 Reconstruction of an Ideal Frequency Representation . . . 38
4.7.2 Short-Time Fourier Transformation (STFT)-based Reconstruction of Time-dependent Harmonic Amplitudes . . . 46
V RAYLEIGH WAVES FOR NONLINEAR MEASUREMENTS . 53
5.1 Theory of Linear Rayleigh Waves . . . 53
5.2 A Model for Rayleigh Waves in Nonlinear Materials . . . 56
5.2.1 Model . . . 56
5.2.2 Discussion . . . 59
5.3 Nonlinear Parameter β_{R} for Rayleigh Waves . . . 62
5.3.1 Derivation of a Nonlinear Parameter β_R . . . 62
5.3.2 Justification and Verification of the Nonlinear Parameter β_R 64
5.4 Further Discussions on the Nonlinear Parameter β_{R} . . . 67
5.4.1 Discussion and Comparison with β . . . 67

5.4.2 Physical Connection between β and β_R 70
5.4.3 A Different Definition for a Nonlinear Parameter for Rayleigh Waves 71
5.5 Summary 72
VI THE NONLINEARITY PARAMETER AND FATIGUE DAMAGE 73
6.1 General Considerations 73
6.2 A Model for the Nonlinear Parameter Depending on the Fatigue Life 74
6.2.1 Contribution from Lattice Elasticity 74
6.2.2 Contribution from Dislocation Monopoles 75
6.2.3 Contribution from Dislocation Dipoles 76
6.2.4 Material Nonlinearity in an Initially Stressed Solid with Dislocations 77
6.3 Discussion 78
VII CONCLUSION 81
Appendices 83
APPENDIX A — NONLINEAR WAVE PROPAGATION 83
APPENDIX B — SIGNAL PROCESSING FOR NONLINEAR MEASUREMENTS 85
APPENDIX C — RAYLEIGH WAVES FOR NONLINEAR MEASUREMENTS 88
REFERENCES 89

LIST OF TABLES

4.1 Comparison of commonly used windows [24]. 26

4.2 Comparison between windowing and pulse inversion. 36

4.3 Reconstruction of ideal frequency representation (1 cycle, $k = [6, 15, 20, 25, 26, 27]$). 42

4.4 Reconstruction of ideal frequency representation (5 cycles, $k = [6, 15, 20, 25, 26, 27]$). 42

4.5 Reconstruction of ideal frequency representation (1 cycle, $k = [6, 15, 20, 25, 26, 27, 41, 50]$). 42

4.6 Reconstruction of ideal frequency representation (5 cycles, $k = [6, 15, 20, 25, 26, 27, 41, 50]$). 43

4.7 Reconstruction of ideal frequency representation (1 cycle, $k = [6, 15, 20, 25, 26, 27, 41, 50, 70, 90]$). 43

4.8 Reconstruction of ideal frequency representation (5 cycle, $k = [6, 15, 20, 25, 26, 27, 41, 50, 70, 90]$). 44

4.9 Condition of matrix $\mathbf{M}$. 44

5.1 Constants used for the simulation (steel). 59

6.1 Values at 100 percent of the total life for stress- and strain-controlled fatiguing for nickel [7]. 79

LIST OF FIGURES

3.1 Principle for nonlinear measurements. 11

3.2 Experimental setup for nonlinear measurements with contact transducers. 12

3.3 Nonlinear measurement with contact transducer, typical signal. . . . 13

3.4 Measuring higher harmonics using laser ultrasound. 14

4.1 Results of the DFT/FFT. 17

4.2 Effect of zero-padding in the frequency domain. 18

4.3 Synthetic signals (blue dashed: signal 1, red solid: signal 2). 21

4.4 Magnitude of DFT in the range between 3 and 12 MHz (blue dashed: signal 1, red solid: signal 2). 22

4.5 Leakage by a rectangular window (principle). 23

4.6 Periodic Extension of a sinusoid not periodic in the observation intervall [9]. 24

4.7 Window properties. 25

4.8 Commonly used windows (time domain, length 41). 26

4.9 The window is weighing the signal. Therefore it influence on the amplitude has to be corrected. 27

4.10 Rectangular window (length 20, f_s=100 MHz). 28

4.11 Minimal attenuation of a frequency component of a signal leaking into frequencies that are $5 \pm 0.5\,\mathrm{MHz}$ away (f_s=100 MHz) considering different windows and different frequency component amplitude ratios (a_1=1 at f_1=5 MHz, a_2=0.05 and a_2=0.005 at f_2=10 MHz). G is a conservative guarantee for the maximum leakage with M=200 and the amplitude ratio a_1/a_2=200. 30

4.12 Nonlinear measurement, DC-offset subtracted, circles are beginning/end of window (red solid: Blackman window, blue dashed: Hanning window; windows are ploted ten times inflated). 34

4.13 Magnitude of windowed signal (red solid: Blackman window, blue dashed: Hanning window). 35

4.14 Signal after pulse inversion (scaled for factor 2). 35

4.15 Max. Leakage from 5.2 MHz into frequency range around 10.4 MHz in dB of first harmonic amplitude (red solid: Blackman window, blue dashed: Hanning window). 36

4.16 Principle of the STFT in the time domain (dashed line: window centered at two different times t_1 and t_2). 47

4.17 Window as smoothing function in the frequency domain ($W_1(\xi)$ wideband, $W_2(\xi)$ narrowband window). 47

4.18 Blackman window (length 301, f_s=500 MHz) for a STFT-based reconstruction of the harmonics (f=5, 10, 15 MHz). 50

4.19 STFT-based reconstruction of slightly time-varying harmonic amplitudes. 51

4.20 STFT of signal $s(t)$ with normalized Blackman window of length 301. 52

5.1 Coordinates for Rayleigh waves. 54

5.2 Spectral velocity amplitudes (1st to 4th harmonic), calculated with 128 harmonics, constants as in Table 5.1. 60

5.3 Waveforms due to nonlinearity on the surface in terms of the horizontal and vertical components of the particle velocity. 61

5.4 Normalized second harmonic velocity amplitude in z-direction, out of model (steel) and measurement (Nickel Base Superalloy). 65

5.5 Normalized third harmonic velocity amplitude in z-direction (model with steel, v_{z1}=constant). 66

5.6 Second harmonic velocity amplitude over first harmonic velocity amplitude squared in z-direction (model with steel) at different propagation distances. 67

5.7 Nonlinear parameter β_{R} for Rayleigh waves dependent on the third order elastic constants A and B (A and B in percent of the values in Table 5.1). 68

5.8 Nonlinear parameter β for longitudinal waves dependent on the third order elastic constants A and B (A and B in percent of the values in Table 5.1). 69

5.9 Ratio β/β_{R} dependent on the third order elastic constants A and B (A and B in percent of the values in Table 5.1). 69

5.10 Second harmonic generation with Rayleigh waves according to [25]. . 70

B.1 Commonly used windows (frequency domain, length 41). 86

C.1 Nonlinear parameter β_{R3} for Rayleigh waves dependent on the third order elastic constants A and B (A and B in percent of the values in Table 5.1). 88

SUMMARY

An effective way to describe changes in the microstructure of a material or to assess fatigue damage at an early stage in fatigue life is by measuring the acoustic nonlinearity parameter β. The nonlinearity parameter is defined for harmonic longitudinal plane waves and it depends on the ratio of the amplitudes of the first harmonic of the exciting signal and the second harmonic. A reliable measurement of the amplitudes of these harmonics is crucial since their amplitude of the second (higher) harmonic is much smaller than the amplitude of the first harmonic.

This research investigates the influence of the apparent nonlinearity that can occur due to the signal processing and shows how this influence can be quantified and minimized to enable a more accurate evaluation of the acoustic nonlinearity parameter.

Furthermore the concept of the nonlinear parameter is extended to Rayleigh surface waves by developing a connection between the harmonic amplitudes and the third order elastic constants, using the approximate model by Zabolotskaya [33].

Finally the problem of modeling the influence of fatigue damage on the nonlinear parameter and the elastic constants is discussed.

The reduction of the processing nonlinearity combined with Rayleigh surface waves - Rayleigh surface waves are more efficient in the detection of fatigue damage initiated and concentrated at the surface - helps improve the prediction of fatigue damage and the remaining life of a sample.

CHAPTER I

INTRODUCTION

Nondestructive Evaluation (NDE) is critical for many high performance components in the aviation, automotive and energy industries. Structural components in these applications often have high loading spectrum, long in-service lives, plus a high demand for safety; material fatigue is often a crucial problem for these structural components.

In metallic materials, the microstructure changes continuously under cyclic loading [28]. First dislocations build up to form substructures such as veins and persistent slip bands on the surface of the material. The stress concentrates on the slip bands, and then develops microcracks that grow under the cyclic loading. Crack initiation takes place near the end of the life of the material and, once initiated, a crack can grow relatively quickly and lead to catastrophic failure.

Therefore it is important to detect cracks in a very early stage or even better, to detect changes in the microstructure before the crack initiation even occurs. A candidate NDE technique for this application is nonlinear acoustic measurements [21].

Unlike linear measurements such as attenuation and the velocity of acoustic waves, nonlinear measurements use the principle that ultrasonic waves generate higher harmonics while propagating through a fatigued material [30, 8, 6]. The reason for this generation of higher harmonics is that the stress-strain relationship becomes (more) nonlinear with increased higher order elastic constants due the material defects. The amplitude of the harmonic waves is directly related to the elastic constants or material properties by the nonlinear acoustic parameter, β. This nonlinear parameter is much more sensitive to microstructure changes (over the fatigue life) of a sample

than linear parameters such as attenuation or the velocity of acoustic waves. Changes in these linear parameters (as a function of fatigue life) are extremely small, and are therefore extremely difficult to measure.

An introduction to linear and nonlinear wave propagation as well as the derivation is described in Chapter II of this thesis. Different measurement setups and techniques for generating and detecting high amplitude ultrasonic waves in order to determine the nonlinear acoustic parameter are presented in Chapter III.

For measuring the nonlinear acoustic parameter β, the absolute amplitudes of the first harmonic[1] and the second harmonic in the wave signal have to be determined where the second harmonic amplitude is extremely small compared to the first harmonic amplitude (typically 40 to 100 times smaller in most metallic materials).

One purpose of this thesis is to develop and investigate different signal processing techniques for determining the harmonic amplitudes from measured transient wave signals as exactly as possible. A variety of candidate signal processing techniques are compared and evaluated. The main focus is on a windowing technique applied for reconstructing absolute amplitudes out of the frequency domain. The requirements for this technique, as well as guarantees of the accuracy of the amplitudes, are discussed.

The nonlinear acoustic parameter in its original form is defined for longitudinal harmonic waves. Chapter V extends the concept of the nonlinear acoustic parameter to Rayleigh surface waves, and derives a corresponding parameter for Rayleigh waves in nonlinear isotropic materials. Rayleigh surface waves have the advantage that their energy is concentrated on the surface — and crack initiation usually occurs at the surface [28] — so they have great promise in delivering more accurate life prediction information. Such a model for the effect of dislocations on the nonlinear acoustic parameter as well as for the development of β over life is shown and discussed in chapter VI.

[1] Throughout the thesis the first harmonic is related to the frequency of the harmonic input signal.

CHAPTER II

WAVE PROPAGATION IN SOLIDS

2.1 Equations of Motion

Starting point for all problems related to wave propagation is the equation of motion, also known as elastodynamic equation.

In linear and nonlinear elasticity, the traction t_i on a plane $n_i x_i = d$ is given by the Cauchy formula

$$t_i = \sigma_{ij} n_j \ , \tag{2.1}$$

where σ_{ij} is the stress tensor.

The balance of linear momentum for a body with volume V and surface S can be expressed as

$$\int_S \sigma_{kl} n_l dS + \int_V \rho f_k dV = \int_V \rho \ddot{u}_k dV \ , \tag{2.2}$$

with ρ representing the material mass density and f_i representing the body force. Gauss' theorem applied to (2.2) leads to

$$\int_V \left(\sigma_{kl,l} + \rho f_k - \rho \ddot{u}_k\right) dV = 0 \ . \tag{2.3}$$

Equation 2.3 has to be fulfilled for any arbitrary body volume V, and therefore the stress equation of motion becomes

$$\sigma_{kl,l} + \rho f_k = \rho \ddot{u}_k \ . \tag{2.4}$$

In the following the body force f_i is always neglected.

2.2 Linear Wave Propagation

It is often more efficient to have the equation of motion given solely in terms of the displacement, u_i (as opposed to (2.4), which contains terms of stress σ_{ij} and displacement u_i). Therefore the relation between stress and displacement has to be used that is directly linked with the stress-strain relationship.

The stress-strain relationship determines whether the wave propagation is linear or nonlinear.

2.2.1 Linear Elasticity

In the case of a homogeneous, isotropic and linear medium the relation between stress and strain is given by Hooke's law,

$$\sigma_{ij} = \lambda \epsilon_{kk} \delta_{ij} + 2\mu \epsilon_{ij} \,, \tag{2.5}$$

where μ and λ are the Lamé constants and ϵ_{ij} is the strain tensor that is related to the displacement u_i by

$$\epsilon_{ij} = \frac{1}{2}(u_{i,j} + u_{j,i}) \,. \tag{2.6}$$

Plugging (2.6) into (2.5) and subsequently into (2.4) with neglected body forces leads to Navier's equations of motion

$$\mu u_{i,jj} + (\lambda + \mu) u_{j,ji} = \rho \ddot{u}_i \,, \tag{2.7a}$$

which reads in vector representation as

$$\mu \nabla^2 \mathbf{u} + (\lambda + \mu) \nabla \nabla \cdot \mathbf{u} = \rho \ddot{\mathbf{u}} \,. \tag{2.7b}$$

The partial differential equation (2.7) is linear due to the unique relation of stress and strain through constant coefficients (λ, μ, ρ). As a result it is satisfied by an harmonic solution, i.e. the propagating wave is harmonic. Therefore waves can be

represented as superposition of independently propagating "monochromatic"' waves.

To solve the partial differential equation (2.7), one applies the Helmholtz decomposition

$$\mathbf{u} = \nabla\varphi + \nabla \times \boldsymbol{\psi}\,, \tag{2.8}$$

which provides a convenient way to uncouple the equation of motion. Equation 2.8 represents the three components of the displacement $\mathbf{u}$ with the four functions φ, ψ_1, ψ_2 and ψ_3. To guarantee the uniqueness of the solution, an additional constraint

$$\nabla \cdot \boldsymbol{\psi} = 0 \tag{2.9}$$

is introduced. Substitution of (2.8) into the displacement equation of motion (2.7) leads to two uncoupled wave equations expressed in terms of the displacement potentials φ and $\boldsymbol{\psi}$:

$$\nabla^2\varphi = \frac{1}{c_{\mathrm{L}}^2}\ddot{\varphi}\,, \qquad \nabla^2\boldsymbol{\psi} = \frac{1}{c_{\mathrm{T}}^2}\ddot{\boldsymbol{\psi}}\,, \tag{2.10}$$

whereas – as shown later – c_{L} represents the wave speed of longitudinal waves and c_{T} the wave speed of vertically and horizontally polarized (transverse) shear waves,

$$c_{\mathrm{L}}^2 = \frac{\lambda + 2\mu}{\rho}\,, \qquad c_{\mathrm{T}}^2 = \frac{\mu}{\rho}\,. \tag{2.11}$$

The inequality $c_{\mathrm{L}} > c_{\mathrm{T}}$ holds always. Both wave speed equations are expressed in terms of density ρ and the Lamé constants μ and λ.

The equation of motion (2.7) can also be formulated using the wave speed for the longitudinal and transversal component,

$$c_{\mathrm{T}}^2 u_{i,jj} + (c_{\mathrm{L}}^2 - c_{\mathrm{T}}^2) u_{j,ji} = \ddot{u}_i\,, \tag{2.12a}$$

or in vector representation as

$$c_{\mathrm{T}}^2 \nabla^2\mathbf{u} + (c_{\mathrm{L}}^2 - c_{\mathrm{T}}^2)\nabla\nabla\cdot\mathbf{u} = \ddot{\mathbf{u}}\,. \tag{2.12b}$$

2.2.2 Linear Wave Phenomena

Linear wave phenomena discussed in this section are based on the plane wave assumption, i. e., assuming a wave with constant properties (ϵ, σ, u) on a plane perpendicular to its direction of propagation $\mathbf{p}$. The mathematical representation of a plane wave is

$$\mathbf{u} = \mathbf{d} f(\mathbf{x} \cdot \mathbf{p} - ct) \,, \tag{2.13}$$

where $\mathbf{d}$ is the unit vector defining the direction of particle motion, and c is either the longitudinal wave speed c_L or the transverse wave speed c_T. By substituting (2.13) into (2.7), one obtains

$$(\mu - \rho c^2)\mathbf{d} + (\lambda + \mu)(\mathbf{p} \cdot \mathbf{d})\mathbf{p} = 0 \,. \tag{2.14}$$

Since $\mathbf{p}$ and $\mathbf{d}$ are two different unit vectors, it can be seen that the two possible solutions that form the basis of wave propagation are either $\mathbf{d} = \pm\mathbf{p}$ or $\mathbf{p} \cdot \mathbf{d} = 0$:

1) $\mathbf{d} = \pm\mathbf{p}$ leads to $\mathbf{p} \cdot \mathbf{d} = \pm 1$. Inspection of (2.14) yields $c = c_\mathrm{L}$ as defined in (2.11). Since $\mathbf{d}$ and $\mathbf{p}$ are linearly dependent, this represents a particle movement in the direction of propagation – a longitudinal or P-wave.

2) $\mathbf{p} \cdot \mathbf{d} = 0$ leads with (2.11) and (2.14) to $c = c_\mathrm{T}$. Hence, the direction of motion is normal to the direction of propagation, and the wave is called a transverse wave. If a two-dimensional plane of propagation is considered (for example, the (x_1, x_2)-plane), a wave with an in-plane displacement (in the (x_1, x_2)-plane) is called an SV-wave (vertically polarized), while a wave with out-of-plane displacement (in the x_3-direction) is called an SH-wave (horizontally polarized).

In a homogeneous, isotropic material, transverse and longitudinal wave speeds are independent of frequency – they are nondispersive.

2.3 Nonlinear Wave Propagation

The assumption of linear elasticity is only an approximation, and all real solids display some degree of nonlinearity. The propagating waves are not harmonic and interact with other waves in the solid (e.g. thermal waves etc.) and distortion also creates higher harmonics. A detailed discussion of those effects can be found in [30].

2.3.1 Strain Energy and Third-order Elastic Constants

The nonlinear effects can be related to the coefficients of the third- and higher-order terms of the strain energy function. Under the assumption that the strain energy is zero before deformation (before the a wave propagates) and assuming zero-initial stress the strain energy function (or strain energy density) can be written as

$$E = \frac{1}{2} C_{ijkl} \epsilon_{ij} \epsilon_{kl} + \frac{1}{3} C_{ijklmn} \epsilon_{ij} \epsilon_{kl} \epsilon_{mn} + \dots \tag{2.15}$$

The C_{ijkl} are the second-order elastic coefficients that are related to the Lamé constants by

$$C_{ijkl} = \lambda \delta_{ij} \delta_{kl} + \mu \left(\delta_{ik} \delta_{jl} + \delta_{il} \delta_{jk} \right) . \tag{2.16}$$

The C_{ijklmn} are the third-order elastic constants in the expansion of the strain energy function.

The nonlinear effects are connected with third-order terms or higher in the strain energy function and therefore the coefficients represent the quantities that determine the nonlinear behavior.

The actual number of independent third-order coefficients necessary to define the properties of a particular medium depends on symmetry. An isotropic material requires three independent third-order coefficients. Third-order elastic constants have widely been discussed and references on this can be found in [30]. A table with commonly used third-order elastic constants is given in [6]. In this research the definition

for isotropic materials following Landau and Lifshitz [17] is used where the third-order elastic constants are defined as A, B and C. The strain energy function for an isotropic material becomes then

$$E = \mu\epsilon_{ik}^2 + (\frac{1}{2}K - \frac{1}{3}\mu)\epsilon ll^2 + \frac{1}{3}A\epsilon_{ik}\epsilon_{il}\epsilon_{kl} + B\epsilon_{ik}^2\epsilon_{ll} + \frac{1}{3}C\epsilon_{ll}^3 + \dots . \tag{2.17}$$

The bulk modulus K can be easily expressed in terms of the Lamé constants λ and μ as

$$K = \lambda + \frac{2}{3}\mu\,. \tag{2.18}$$

2.3.2 Nonlinear Wave Equation

The nonlinear wave equation is calculated by using the relationship between the stress σ_{kl} and the strain energy function E,

$$\sigma_{kl} = \frac{\partial E}{\partial u_{k,l}}\,, \tag{2.19}$$

as well as the approximation between the strain ϵ_{ij} and the displacement u_i,

$$\epsilon_{ij} = \frac{1}{2}\left(u_{i,j} + u_{j,i}\right)\,. \tag{2.20}$$

Everything plugged in the equation of motion (2.4) leads to a quite lengthy term.

In the 1-d case of a plane longitudinal wave propagating in x-direction the equation of motion becomes

$$\frac{\partial^2 u_x}{\partial t^2} = c_l^2\left(1 - \beta\frac{\partial u_x}{\partial x}\right)\frac{\partial^2 u_x}{\partial x^2} \tag{2.21}$$

when the third order constants are the highest ones considered. The parameter β is a measure for the nonlinearity and is therefore also called nonlinear parameter.

2.4 Nonlinear Parameter β

The nonlinear parameter β can be represented in terms of the elastic constants of a material as well as in terms of its harmonic amplitudes generated by a single frequency harmonic wave. Therefore β is used to track changes in the material.

2.4.1 Material Property Dependency of β

For the 1-d case (longitudinal, bulk) above with an isotropic material the nonlinear parameter β in terms of the elastic constants is given as

$$\beta = -\frac{3(\lambda + 2\mu) + (2A + 6B + 2C)}{(\lambda + 2\mu)} \tag{2.22}$$

with the elastic constants λ, μ from the linear theory and the third order elastic constants A, B, C. This expression is only valid for the assumption of zero-initial stress. Otherwise the initial stress in the solid has to be added to denominator in Equation (2.22).

2.4.2 β in Terms of Harmonic Amplitudes

Assuming an input wave of the form $u(x = 0, t) = u_0 cos(\omega t)$ an approximation for the solution of Equation (2.21) is calculated by using a perturbation method [5, 8, 30]. It is given to second order in displacement as

$$u(x,t) = \frac{1}{8}\beta k^2 u_0^2 x + u_0 cos(kx - \omega t) - \frac{1}{8}\beta k^2 u_0^2 x\, cos(2(kx - \omega t)) + \dots , \tag{2.23}$$

where k is the wavenumber, ω the circular frequency and x the distance from the source. The calculation of this solution can be found in Appendix A.1.

The nonlinearity does not only generate higher harmonics, but also a DC part. The nonlinearity parameter can either be determined by the ratio of the harmonic amplitudes or by the DC part. A determination via the DC part is possible but it requires a low frequency transducer and the separation from other offsets can be difficult.

Following Equation (2.23) β is determined in terms of the first and second harmonic amplitude, A_1 and A_2 as

$$\beta = \frac{8A_2}{k^2 A_1^2 x}\,. \tag{2.24}$$

Note that β is not just the ratio between the second harmonic amplitude A_2 and the first harmonic amplitude squared A_1^2. The sign of β is not very important to show

changes in the material properties, it is far more a result of the exact definition.

More about nonlinear acoustics and nonlinear waves can be found in [8], [6], [22] and [30].

CHAPTER III

NONLINEAR MEASUREMENTS

The purpose of this chapter is to give a short overview over the techniques used to track changes in the third order elastic constants by determining the nonlinear parameter β. The techniques presented here use ultrasound produced and measured either by ultrasonic transducers and or a laser.

3.1 Principle of Nonlinear Measurements

In the previous chapter the nonlinear parameter β is given in terms of harmonics generated by the nonlinearity from an harmonic input wave. This is also the principle used for the measurement. A harmonic wave input into the nonlinear material at one side of a specimen generates an output of additional higher harmonics, as indicated in Figure 3.1.

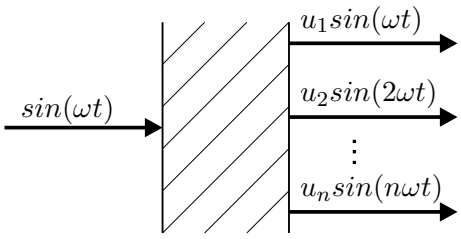

Figure 3.1: Principle for nonlinear measurements.

The use of frequencies in the range of several MHz (ultrasound) has a physical reason. Following Equation (2.23) with $k = \omega/c$, it can seen that higher frequencies increase the absolute value of the higher harmonic amplitudes. The higher harmonics are also proportional to the input amplitude u_0.

Effects like scattering by the geometry of the sample, dispersion due to the finite size

of transducers and attenuation in the material change also the harmonic amplitudes and have to be kept in mind when doing measurements.

3.2 Measurement of the Nonlinear Parameter using Contact Transducers

A typical setup for nonlinear measurements (bulk longitudinal waves) using contact transducers is given in Figure 3.2. Transducer and receiver are slightly pressed on the opposite sides of the surface of the flat sample. Between transducer/receiver and sample is an oil couplant to couple the ultrasound better into the specimen. The rubber ensures uniform contact of the transducer and receiver with the sample. The piezo-electric load cell allows to measure any changes in the force that is applied to transducer/receiver since a change in the force changes the amplitude of the waves coupled into the material.

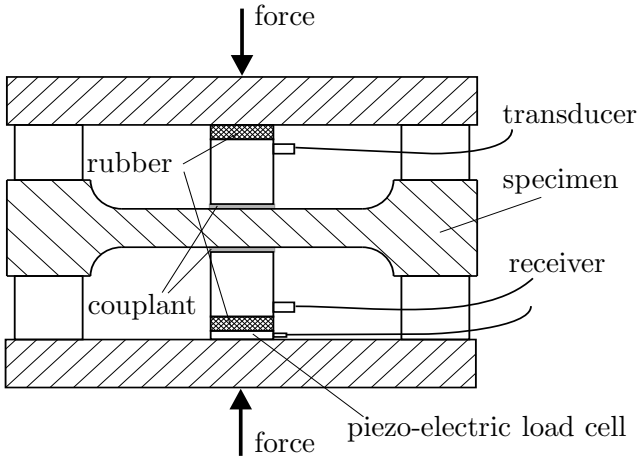

Figure 3.2: Experimental setup for nonlinear measurements with contact transducers.

A typical signal measured with the receiver in the setup above is given in Figure 3.3. Nine cycles of a sinusoid with 5.2 MHz are used as an input. The first wave packet is the transmitted signal, the followings are due to reflections in the sample (thickness 0.25 inches) that can superimpose the transmitted signal if the input signal is too long. Therefore the length of the signal that can be used for determining the

β is limited. The reflected and transmitted waves interact in the material due to the nonlinearity, so that they cannot be removed by considering only the reflection at the boundaries.

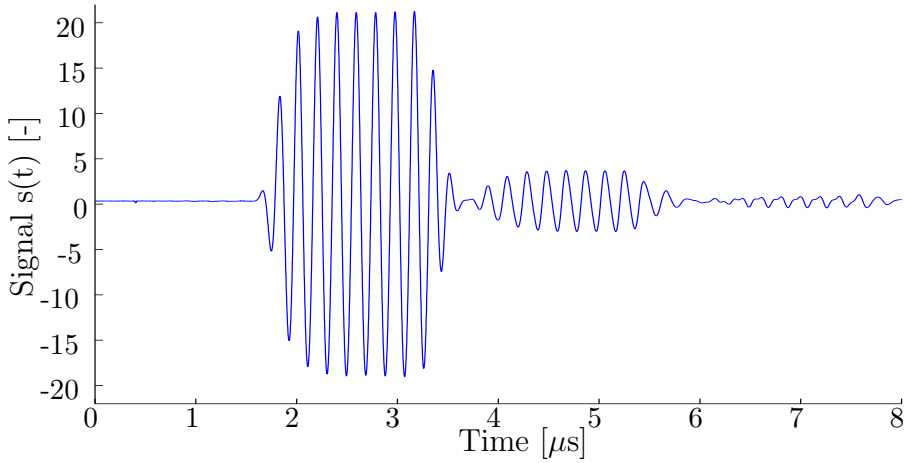

Figure 3.3: Nonlinear measurement with contact transducer, typical signal.

Every transducer/receiver has a characteristic frequency magnitude relationship (e.g. band limitation) that has to be considered. For example the DC part described in the previous chapter can often not be seen in the frequency domain or is too small due to the receiver characteristic.

3.3 Measurement of the Nonlinear Parameter using Laser Ultrasound

Another technique to measure ultrasonic waves is by using a laser interferometer. Using a heterodyne interferometer where the interference between a laser beam reflected on the surface of the specimen and a reference beam allows to measure the particle velocity on the surface [12].

In [10] higher harmonics of Rayleigh waves, generated due to the nonlinearity of the specimen, are measured by this technique. The principle setup is sketched in Figure 3.4. If the wedge is designed properly, it ca be shown [31] that only Rayleigh waves are generated; also see [10] for details.

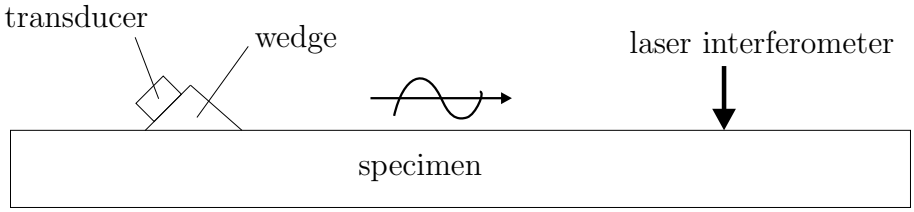

Figure 3.4: Measuring higher harmonics using laser ultrasound.

In a later chapter it is investigated how those Rayleigh waves can be used to determine the change in the third order elastic constants of the material.

CHAPTER IV

SIGNAL PROCESSING FOR NONLINEAR MEASUREMENTS

4.1 The Discrete Fourier Transform

The discrete Fourier Transform (DFT) is a very efficient and powerful tool for representing time signals in the frequency domain. Both, the time and frequency domain are uniformly discretized and limited to a certain time and frequency range, respectively.

4.1.1 Definition

The *discrete Fourier transform* of a (time) sequence[1] $x[n]$ that is zero outside the range $n = 0, \ldots, N-1$ is defined as

$$X[k] = \sum_{k=0}^{N-1} x[n] W_N^{kn}\,, \tag{4.1}$$

where

$$W_N = e^{-i(2\pi/N)} \tag{4.2}$$

is a complex sinusoid, sometimes also called phase factor. The $2\pi/N$ in W_N is the discretization width of the normalized frequency. Since N data points are involved it is also called N-point DFT.

In contrast to the continuous Fourier Transform [4], the existence of the DFT is always guaranteed since finite length sequences (with finite values) are always summable what makes the use of the DFT very convenient.

[1] Small letters denote signals in the time domain and capital letters signals in the frequency domain. Squared brackets '[ ]' are used to indicate the discrete nature of a signal.

As a synthesis formula, the *inverse discrete Fourier transform (IDFT)*, represents the sequence $x[n]$ as a superposition of infinitesimal small complex sinusoids of the form

$$x[k] = \frac{1}{N} \sum_{k=0}^{N-1} X[k] W_N^{-kn}, \tag{4.3}$$

with $X[k]$ determining the relative amount of each complex sinusoidal component. Consequently the Fourier transform can be understood as a measure for "how much" oscillations at the discrete frequency k there is in the time sequence $x[n]$ [20]. This allows to determine the amplitudes of different frequency components of a signal.

The general existence of the DFT also guarantees the existence of the IDFT. Whether the DFT and its inverse are unique is another question, yet.

4.1.2 Nyquist Sampling Theorem

The uniqueness of the DFT is directly linked to the sampling and the bandwidth or frequency content of the measured physical signal.

The *Nyquist Sampling Theorem* gives a necessary condition to reconstruct a continuous signal from its discrete representation: the sampling frequency f_s has to be at least twice the highest frequency component of the continuous signal to avoid aliasing. Aliasing leads to a misinterpretation of higher frequency components ($> f_s/2$) as lower frequency components in the frequency domain. A very detailed explanation of the Nyquist Sampling Theorem and its discussion can be found in [24].

For the practical use, it is just important to know that as long as the Nyquist Sampling Theorem is full filled, every signal has a unique frequency representation and it can be reconstructed exactly from its frequency representation. If necessary, higher frequencies have to be filtered out before doing a frequency analysis.

4.1.3 Fast Fourier Transform (FFT)

The fast Fourier transform algorithms are a particularly efficient class of algorithms for the digital computation of the N-point DFT. In general the input and output keeps to the definition for the DFT given in Equation (4.1), only the indices are sometimes slightly different, e.g. in Matlab they run from 1 to N.
The IDFT can be easily calculated using the duality property of the DFT (see Properties of the DFT) and the DFT algorithm, often already implemented as a command.

The assignment of frequencies to the discrete indices of the DFT has to be done carefully. As shown in Figure 4.1 the DFT covers a range of $0 \leq \omega < 2\pi$ of the normalized frequency with its discrete index. From the definition of the DFT (4.1) it can be seen that the DFT is periodic with 2π so that the DFT can be shown over the very common range between $\pm\pi$ or $\pm f_s/2$. Especially this step is very crucial.

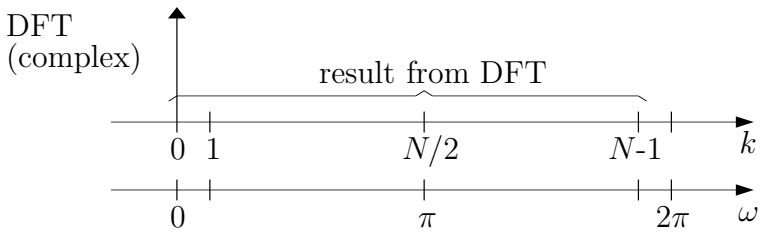

Figure 4.1: Results of the DFT/FFT.

The FFT algorithms are most efficient when N is a power of 2. However, if calculation time is not very relevant other aspects for the signal length N have to be considered.

4.1.4 Zero-Padding

The signal length N can be varied by extending a signal with zeros, known as zero-padding. For measured signals (causal) this is done by appending zeros to the end of the original signal.

The effect is shown in a simple example. The (time) signal is given as $x[n] = 1$, $n = 0, 1, \ldots, 4$. Then the DFT is performed with and without appending five zeros at the

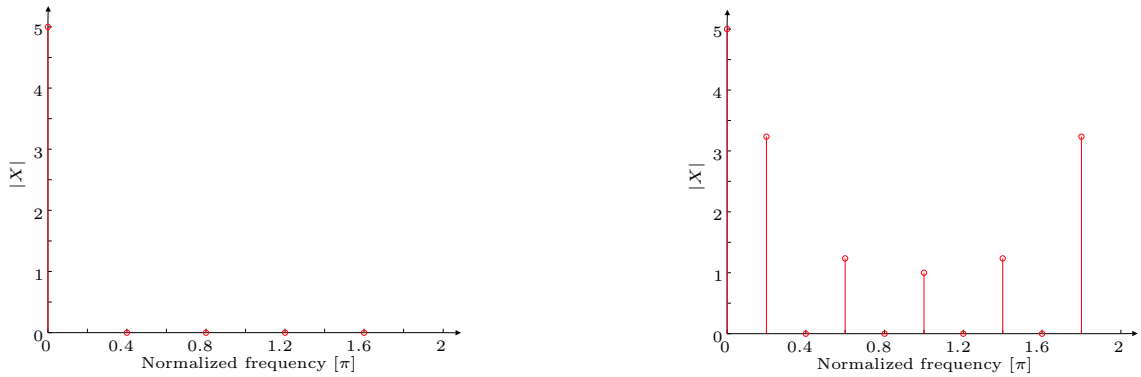

(a) Without zero-padding.

(b) With zero-padding (5 zeros).

Figure 4.2: Effect of zero-padding in the frequency domain.

end of the signal. The result in terms of the magnitude of the DFT is shown in Figure 4.2.

By zero-padding one can see additional peaks in the frequency domain. Since there is no information added by appending zeros to the signal, the only effect of the zero-padding is that the sampling of the frequency domain has become finer. The *Zero-Padding Theorem* states that zero padding in the time domain corresponds to an ideal interpolation in the frequency domain [27]. Therefore zero-padding is a useful tool to get frequency representations for additional discrete frequencies.

It is obvious that one should make sure that the discrete frequencies match the frequencies of interest in the signal x, in the current case the frequency of the harmonics in the signal. This can be done by appending so many zeros to a signal of length N_s such that the frequency of the first harmonic f_1 is an integer multiple of $f_s/(2(N_s + N_0))$, where N_0 is the number of the appended zeros.

4.1.5 Properties of the DFT

In this section a selection of properties of the DFT are listed that are important for this research.

All properties are given for the sequence $x[n]$, that is zero outside the time index range $0 \leq n \leq N-1$ and its DFT $X[k]$ with the frequency index range $0 \leq k \leq N-1$. The same applies for the sequences $x_1[n]$ and $x_2[n]$ and their DFT, respectively.

- **Linearity:**

$$ax_1[n] + bx_2[n] \overset{\mathcal{DFT}}{\leftrightarrow} aX_1[k] + bX_2[k]\,, \tag{4.4}$$

  where a and b are arbitrary scalars.

- **Duality**[2]:

$$x[n] \quad \overset{DFT}{\leftrightarrow} \quad X[k] \tag{4.5}$$

$$\frac{1}{N}X[((-n))_N] \quad \overset{DFT}{\leftrightarrow} \quad x[k]\,. \tag{4.6}$$

  Allows to calculate the IDFT by using a FFT algorithm.

- **Circular Shift of a Sequence:**

$$x[((n-m))_N] \overset{\mathcal{DFT}}{\leftrightarrow} W_N^{km}X[k] \tag{4.7}$$

$$W_N^{-ln}x[n] \overset{\mathcal{DFT}}{\leftrightarrow} X[((k-l))_N]\,, \tag{4.8}$$

  where $((n-m))_N := ((n-m) \,\text{modulo}\, N)$.

  A circular shift in the time domain by m samples (time delay or time advance depending on the sign of m) corresponds in the frequency domain to a multiplication by the linear phase factor $W_N^{km} = e^{-j(2\pi k/N)m}$. A similar relation is valid for a shift in the frequency domain,

[2]Note that the left side is always the time domain, the right side the frequency domain.

- **Circular Convolution:**

$$x_1[n]x_2[n] \overset{\mathcal{DFT}}{\leftrightarrow} \frac{1}{N}\sum_{l=0}^{N-1} X_1[l]X_2[((k-l))_N] \tag{4.9}$$

$$\sum_{m=0}^{N-1} x_1[m]x_2[((n-m))_N] \overset{\mathcal{DFT}}{\leftrightarrow} X_1[k]X_2[k]\,. \tag{4.10}$$

Multiplication in the time domain corresponds to a circular convolution in frequency domain. It is a basic property for the understanding of windowing effects. Reciprocal, a multiplication in frequency is a convolution in time.

A helpful formula for calculating the circular convolution using the FFT is given by

$$x_1[n]x_2[n] \overset{\mathcal{DFT}}{\leftrightarrow} \frac{1}{N} IFFT(FFT(X_1[k]) * FFT(X_2[k]))\,. \tag{4.11}$$

- **Symmetry Properties:**

The symmetry properties are given for real signals: the real part of the frequency representation is symmetric, its imaginary part antisymmetric.

$$x[n] \text{ is real } \overset{\mathcal{DFT}}{\leftrightarrow} \begin{cases} X[k] = X^{\star}[((-k))_N] \\ Re\{X[k]\} = Re\{X[((-k))_N]\} \\ Im\{X[k]\} = -Im\{X[((-k))_N]\} \end{cases}. \tag{4.12}$$

4.2 DFT of Harmonic Signals - Demonstration Example

The overall goal of nonlinear measurements is the determination of the amplitudes of harmonic frequency components in the measured signal. To separate the different frequencies a transformation in the frequency domain is done via the DFT. The idea is that the amplitudes of the frequency components can there be determined.

The following example will give an idea what happens when just a DFT is applied to a harmonic signal. Given are two synthetic signals, signal 1 and signal 2, as shown in Figure 4.3.

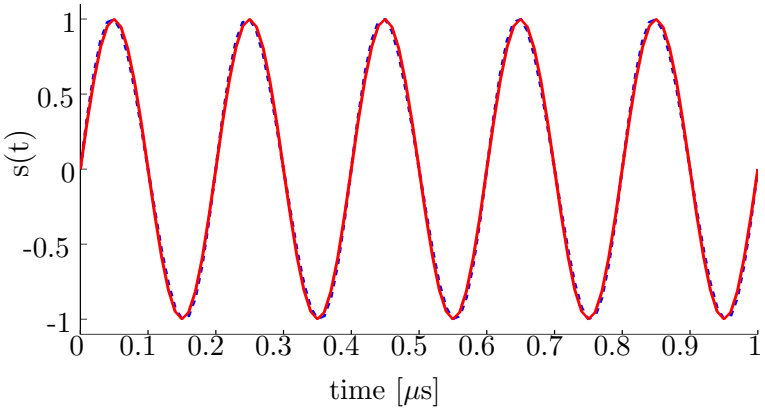

Figure 4.3: Synthetic signals (blue dashed: signal 1, red solid: signal 2).

Signal 1 and 2 are both the sum of two sinusoids of the form,

$$s(t) = a_1 sin(2\pi f_1 t) + a_2 sin(2\pi f_2 t)\,, \tag{4.13}$$

with the frequencies f_1=5MHz and f_2=10MHz and the amplitude a_1=1. The only difference is in the amplitude a_2 where signal 1 has the value 0.05 and signal 2 the value 0.005. Both signals are sampled with f_s=100MHz, the time is chosen such that five cycles of the lower frequency sinusoid can be seen. The magnitudes of the DFT (with very long zero-padding) of the two signals are shown in Figure 4.2.

Intuitively one expects a peak at 5 MHz and a smaller one at 10 MHz. However,

there is no peak at 10 MHz and there are lots of other peaks or far more ripples. In signal 1 there seems to be a peak near 10 MHz, in signal 2 a peak at this frequency can hardly be seen. A close look to the 5 MHz frequency shows that there is not even a peak exactly at 5 MHz. With the selected zero-padding for signal 1 is the peak at 4.966 MHz and for signal 2 at 4.970 MHz, although the 5 MHz component in both signals is the same. (Note that a rectangular window is used in this example.)

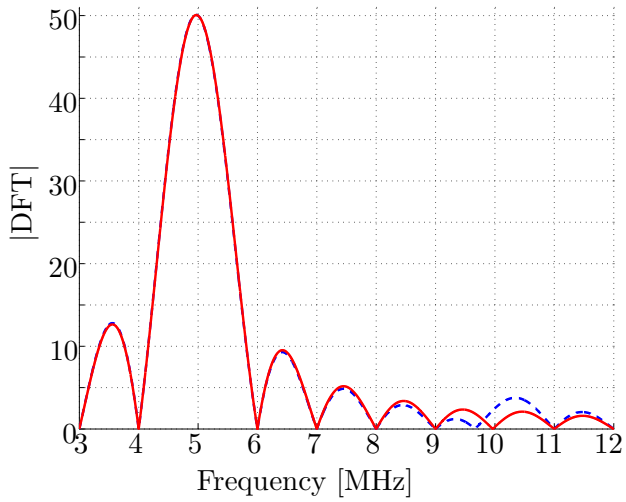

Figure 4.4: Magnitude of DFT in the range between 3 and 12 MHz (blue dashed: signal 1, red solid: signal 2).

This example shows that there are other effects not yet considered and that different frequency components influence each other.

4.3 Windows for Harmonic Analysis

The effects seen in the example are due to windowing. This section describes these effects, introduces some windows and shows how to minimize windowing effects, in particular for the reconstruction of harmonic signal amplitudes for nonlinear measurements. Also explicit recommendations for the use of windowing for nonlinear measurements are given. As an additional reference for this chapter [9] is recommended.

4.3.1 Spectral Leakage

In the definition of the DFT (section 4.1.1) the time sequence $x[n]$ is set to zero outside a certain range $0 \leq n \leq N-1$. This corresponds to cutting out this range of an infinitely long signal or weighing it with a rectangular window,

$$w_{rect}[n] = \begin{cases} 1, & 0 \leq n \leq N-1, \\ 0, & \text{otherwise} \end{cases} .$$

Therefore *every DFT includes windowing due to the finite length of the time signal.*

From the DFT properties in section 4.1.5, Equation (4.10), follows that windowing in the time domain corresponds to a circular convolution in the frequency domain:

$$x[n]w[n] \overset{\mathcal{DFT}}{\leftrightarrow} \frac{1}{N} \sum_{l=0}^{N-1} X[l]W[((k-l))_N] . \tag{4.14}$$

The principle is shown in Figure 4.3.1, where the circular convolution of an ideal frequency representation of an harmonic signal (2 harmonics) at the frequency f_2 is calculated. The window is centered at f_2 (corresponding to a discrete frequency index k) and the product of the peaks of the ideal frequency representation are multiplied with the window, and summed up. This sum is the value for the circular convolution at the frequency f_2. Note that in general the frequency components and the window have complex values.

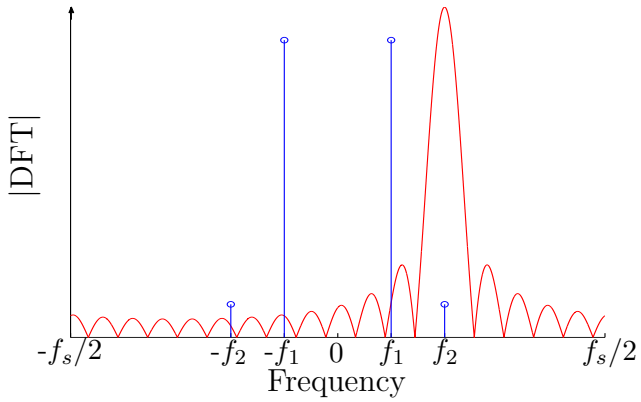

Figure 4.5: Leakage by a rectangular window (principle).

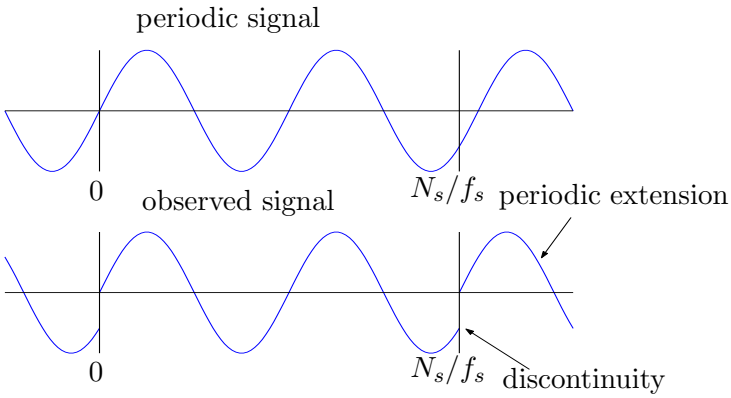

Figure 4.6: Periodic Extension of a sinusoid not periodic in the observation intervall [9].

The contribution from frequencies other than the frequency where the window is centered is called spectral leakage and is responsible for incorrect amplitudes.

Leakage does not only occur from other frequencies, but also from the frequency itself by its negative or positive counter part, respectively.

Another more intuitive approach to spectral leakage can be seen in the time domain. Following [9], sines and cosines with periods equal to an integer submultiple of N_s/f_s seconds form an orthogonal basis set for the continuous signal extending over N_s/f_s seconds. Signals with frequencies other than those of the basis set are not periodic in the observation window. The periodic extension of those signals exhibits discontinuities at the boundary of the observation window that are responsible for the spectral leakage over the entire basis set. This principle is shown in Figure 4.6.

4.3.2 Commonly used Windows

Beside the rectangular window there exists other windows that show useful properties. This research considers the commonly used ones[3].

The main characteristics of windows for harmonic analysis are given by the main lobe

[3]There are many constructed windows for very specific purposes, but "in general the constructed windows tend not to be good windows, and occasionally are very bad windows."[9]

width and the (relative) peak side lobe amplitude as pictured in Figure 4.7. Those properties together with the position of zeros and the amplitude decay in the frequency domain are relevant for where leakage can occur and how high the amount of leakage can be.

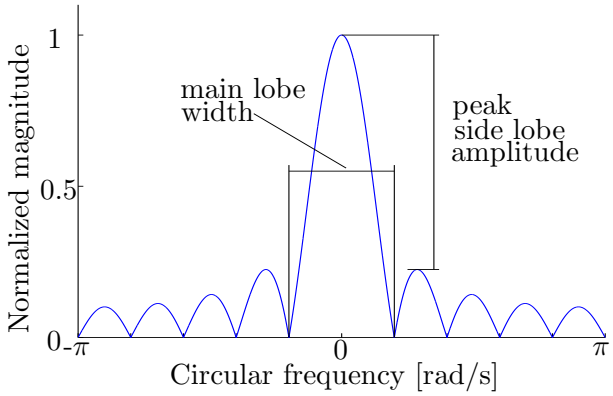

Figure 4.7: Window properties.

The main lobe width is a measure for whether frequencies can be separated. If the amplitude of the frequency components is quite different (as in nonlinear measurements) the (relative) peak side lobe amplitude has also to be considered. The zeros indicate frequencies that do not leak at all in the center frequency of the window. Remember that the frequencies of the window are relative to the center frequency since the window is shifted. Finally, the amplitude decay determines how frequencies that are further away play a role for the leakage.

The connection between the window length M (and therefore also the considered signal length) and the main lobe width as well as the relative peak side lobe amplitude for different windows is given in Table 4.1. It can be seen that the wider the main lobe, the higher the peak side lobe amplitude. The main lobe width is inversely proportional to the window length M.

Figure 4.8 shows the windows from Table 4.1 in the time domain with $M = 41$ (The length 41 is chosen only for presentation purposes.) It can be seen that the signal

Table 4.1: Comparison of commonly used windows [24].

Type of Window	Peak Side Lobe Amplitude (relative) [dB]	Approximation Width of Main Lobe [rad/s]
Rectangular	-13	$4\pi/(M+1)$
Bartlett	-25	$8\pi/M$
Hanning	-31	$8\pi/M$
Hamming	-41	$8\pi/M$
Blackman	-57	$12\pi/M$

near the beginning and end of the window is less weighted than in the center (except for the rectangular window). The effect is a smoothing of the signal at the beginning and the end and a reason of the better performance of the corresponding windows.

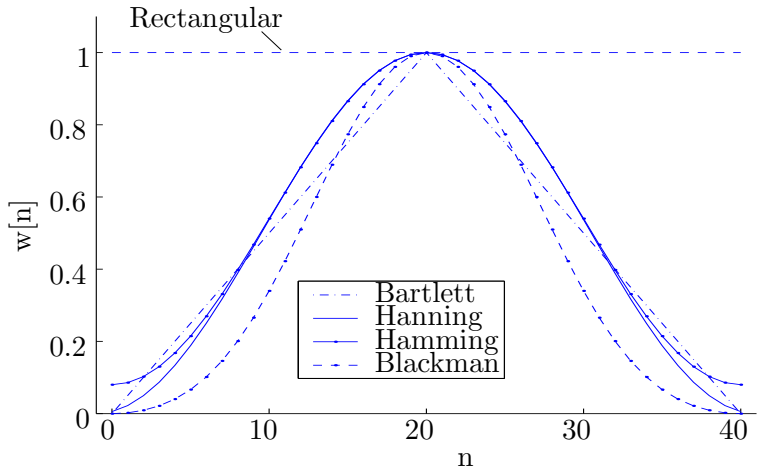

Figure 4.8: Commonly used windows (time domain, length 41).

The exact formulae for the windows as well as their magnitude-frequency plots can be found in the appendix B.1.

4.3.3 Correction of the Amplitude for Windows

As one can see from Figure 4.8, windowing changes the average amplitude of a signal. Additionally the amplitude in the frequency domain depends on the window length. Therefore the magnitude given by the frequency representation has to be correct in

order to reconstruct the amplitudes of the frequency components.

A correction for the energy in the signal is inappropriate since here the interest does not lie in the energy but in the amplitudes. For correcting the influence of the window on the amplitudes, the frequency representation has to be divided by the following correction factor,

$$c_{win} = \frac{1}{2} \sum_{n=0}^{M-1} w[n] \tag{4.15}$$

The sum of the window samples considers the specific window structure or the weighing of the time samples respectively. The factor two is included since the energy of one frequency component is distributed to its positive and negative frequency. Note that the correction factor c_{win} does not correct for leakage.

The correction factor is again illustrated in Figure 4.9. Considered is a sinusoidal signal with a constant amplitude and the window that is applied to it. In the DFT, each sample multiplied by a phase factor is summed up (see Equation (4.1), therefore also the dependency of the magnitude of the DFT on the length of the signal becomes obvious. The window works now as a weighing function that weighs every sample with a value between zero and one. The correction factor corrects for this effect by dividing through the sum of all weighing values.

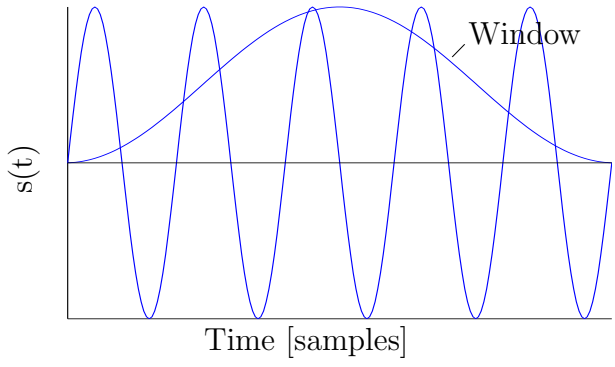

Figure 4.9: The window is weighing the signal. Therefore it influence on the amplitude has to be corrected.

4.3.4 The Rectangular Window

The rectangular window has a special property: its frequency representation is zero for frequencies that are integer multiples of $f_s/(2M)$ [3]. An example for a window length of M=20 and the sampling frequency f_s=100 MHz is given in Figure 4.10.

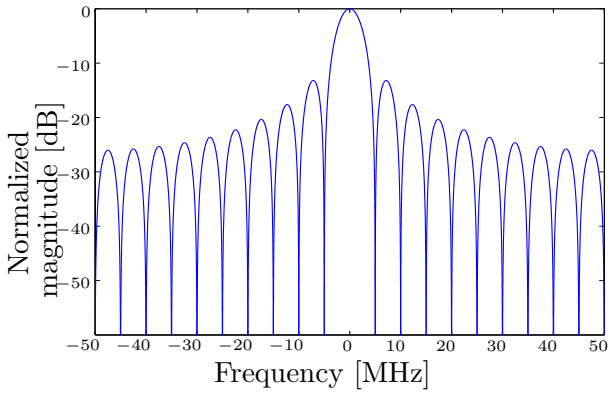

Figure 4.10: Rectangular window (length 20, f_s=100 MHz).

In the case of harmonic signals, this property can be used to get no leakage at the harmonic frequencies.

However, there are strict limits in the use of this property.

1. The frequency of the first harmonic has to be known very exactly; and
2. the equation $f_1 = f_s/(2M)$ has to hold.

Slight deviations of the harmonic frequency can cause big errors, since the slope of the magnitude near the zeros is very high (see Figure 4.10). Considering the synthetic signal 2 from the example in Section 4.2 with M=100 and using the highest peak for getting the first harmonic frequency f_{1r} out of the DFT and taking the corrected magnitude at twice the frequency f_{1r} delivers the amplitude 0.0033 instead of the correct amplitude of 0.005 although the frequency is only slightly different (4.970 MHz instead of 5 MHz). With a real signal this might even be worse.

4.3.5 How to Chose a Window

Windows other than the rectangular window have an overall better performance. However there is no more analytical equation for the location of the zeros.

Figure 4.11 shows the minimal attenuation of a frequency component of a signal (sampling frequency f_s=100 MHz) leaking into a frequency range of 5 ± 0.5 MHz away depending on the considered signal or window length. This is shown for different windows. Additionally the amplitude ratios from first (f_1=5 MHz) to second (f_1=5 MHz) harmonic amplitude (a_1/a_2=20 and a_1/a_2=200) of the two signals in the example in section 4.2 are given. At M=200, for example, when using a Blackman window and using it with a signal that has the amplitude ratio a_1/a_2=200, then G is a conservative guarantee for the maximum leakage from the first harmonic (a_1) into the second harmonic amplitude (a_2). Note that G is a ratio between a_2 and the leakage from a_1 and gives the maximum leakage from the first harmonic to the second harmonics in dB of the second harmonic.

If the range for the leakage is reduced, the estimation for the leakage will become less conservative. Though the interest lies in determining peaks and therefore a frequency range should be considered for the leakage. The estimation is alway conservative. First, it is generated by taking the maximum of the absolute values of the windows in the specified frequency range and second, frequency representations are in general complex.

Figure 4.11 is a tool that guarantees a limit for the maximum leakage. Furthermore it shows the dependency of leakage with the amplitude ratio, the signal/window length and the window type. It also shows that there is a minimum signal length depending on the amplitude ratio.

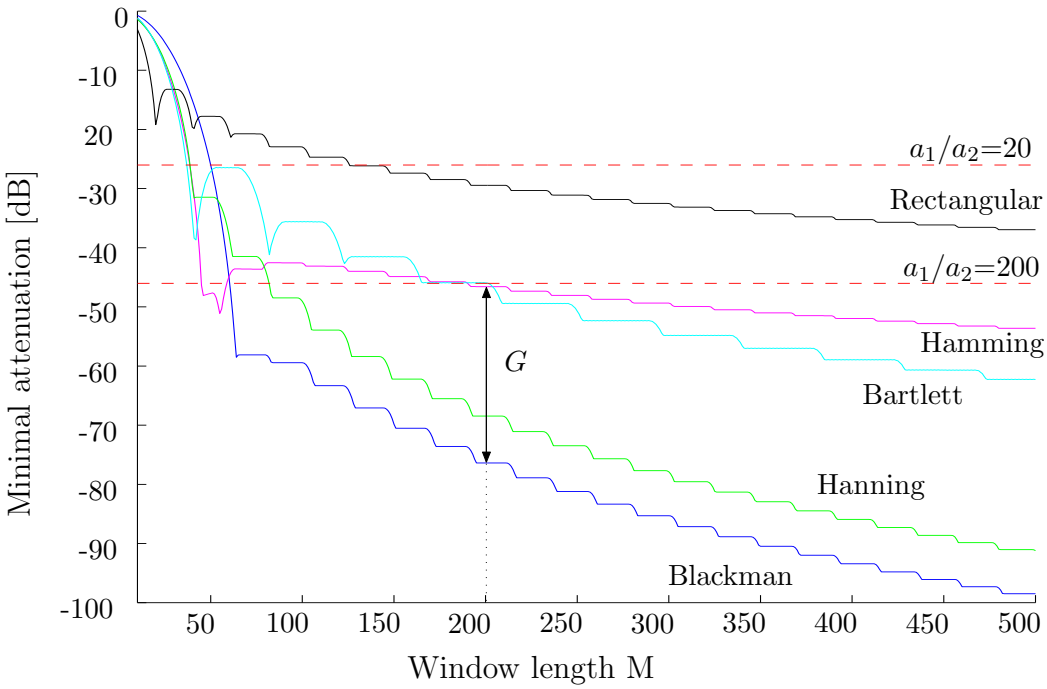

Figure 4.11: Minimal attenuation of a frequency component of a signal leaking into frequencies that are 5 ± 0.5 MHz away (f_s=100 MHz) considering different windows and different frequency component amplitude ratios (a_1=1 at f_1=5 MHz, a_2=0.05 and a_2=0.005 at f_2=10 MHz). G is a conservative guarantee for the maximum leakage with M=200 and the amplitude ratio a_1/a_2=200.

4.3.6 Multiple Windows

The use of multiple windows is not recommended since in general either the main lobe width increases and/or the attenuation decreases. Also signal envelopes have a window effect that deteriorates the performance of the used window. If necessary, the influence of the envelope on the harmonic amplitudes has to be corrected together with the window by using $\overline{w}[n] = window[n] \times envelope[n]$ for the correction factor. If the different frequencies have different envelopes, each frequency component has to be corrected separately. In nonlinear measurements this is always the case due to the quadratic dependency between the harmonic amplitudes.

4.3.7 DC Part and Windowing

The DC part of a signal is often due to the measurement equipment and can easily be removed for harmonic signals by subtracting the mean of the signal. From a windowing point of view it is very useful to remove the DC part since it appears as a peak at $f = 0$ and can therefore also be responsible for leakage (see Figure 4.3.1).

However, if windowing is used in such a way that leakage from one harmonic to the other is below a certain dB-value, then this is also the case for the DC part. Especially for the second harmonic, the DC part is two times the first harmonic frequency f_1 away and should therefore hardly leak into the second harmonic if the DC part is not too big.

Evaluating the DC part itself is better done for harmonic signals by calculating the mean value since the first harmonic will leak from its peak at the positive as well as from its peak at the negative negative frequency. Due to the symmetry of the signal and the window, some parts of the leakage from the positive and negative frequency cancel out.

4.3.8 Rules of Thumb

The following rules of thumb are a result from the previous sections.

1. Subtract the mean value of the signal that is due to the measurement equipment and/or the nonlinearity. Use only the part of the signal where the input into the system is zero to remove the DC part of the equipment.

2. Choose a range of the signal where the amplitude is constant (steady state) to exclude any transient behavior from the equipment.

3. Use only full cycles of the signal to reduce leakage.

4. The longer the signal the smaller the leakage.

5. For long signals (big window length M), use the Blackman window since it has the highest side lobe attenuation of the discussed windows.

6. For short signals (short window length M), use the Hanning window as a trade off between main lobe width and attenuation.

7. Make an estimation how much leakage is possible depending on the signal length and the estimated amplitude ratio.

4.4 Filtering for Harmonic Amplitudes

One simple approach for determining the harmonic amplitudes is by using a bandpass filter for the specific harmonic frequencies and measuring the harmonic amplitudes in the time domain.

However, the properties of the signal result in quite strict requirements for the filter design:

1. The harmonic frequencies are very close to each other in relation to the sampling frequency (e.g. in the example earlier on, the distance is 5 MHz and the sampling frequency 100 MHz). This creates the need for a relatively sharp transition from the stopband to the passband.

2. The amplitude ratio between the harmonic amplitudes is relatively big. Consequently the attenuation in the stopband has to be accordingly big.

Those requirements result (in general) in quite long filters, eventually even longer than the signal itself. Since the settling time of digital filters is half the filter length (in samples) this approach is in general not helpful.

One possibility consists in designing a filter that filters out specific frequencies (the other harmonics) rather than whole frequency bands. Though, with standard filter

design algorithms this is not possible. Considering this windowing seems to be a far more appropriate approach.

4.5 Pulse Inversion

Pulse inversion is a method to extract the second harmonic amplitude in nonlinear measurements. It is explained and successfully demonstrated in [23] and goes originally back to medical ultrasonic imaging [16].

The method consists of superposing two transmitted waves of incident phase 0 and 180 degrees. When the transmitted wave is a cosine of the form $u_{0i}cos(\omega t)$ then the distance dependent transmitted wave is given by

$$u(x,t) = \frac{1}{8}\beta k^2 u_0^2 x + u_0 cos(kx - \omega t) + \frac{1}{8}\beta k^2 u_0^2 x cos(2(kx - \omega t)) + \dots . \quad (4.16)$$

From Equation (4.16) it can be easily seen that the first harmonic cancels out when the two transmitted waves of incident phase 0 and 180 degrees are superimposed. The second harmonic doubles and the DC part can be removed by subtracting the mean value of the signal.

The method can even be applied for short pulses where the signal is too short for other methods. This is the main advantage of this method and can therefore be applied to thin samples.

The main drawback lies in the additional effort of the measurement. Not only are two measurements needed, but also the electronic equipment has to be quite precise for phase-shifts or the beginning of the two signals has to be determined by correlation and the phase shift has to be performed by signal processing.

In the next section, this is discussed in more detail using measured signals and comparing it to the windowing method.

4.6 Example

The purpose of this section is to compare different signal processing methods. In the example (bulk longitudinal), a real signal from a nonlinear measurement using contact transducers is used to compare windowing and pulse inversion in extracting the harmonic amplitudes. As seen earlier, filtering is not very appropriate and the reconstruction of the ideal frequency representation is very limited.

The starting point is a signal where the DC-offset is removed by subtracting the mean over the beginning of the signal, before any harmonics can be seen. Figure 4.12 shows such a signal where 9 cycles of a sinusoid are used for the input transducer. A longer input signal would cause an overlapping with the reflected signal due to the sample thickness. Following the rules of thumb (subsection 4.3.8) only a the part of the signal where the amplitude stays almost constant is used. The beginning and end, in the Figure marked with circles, are chosen such that only full cycles of the signal are used. The number of cycles is as high as possible.

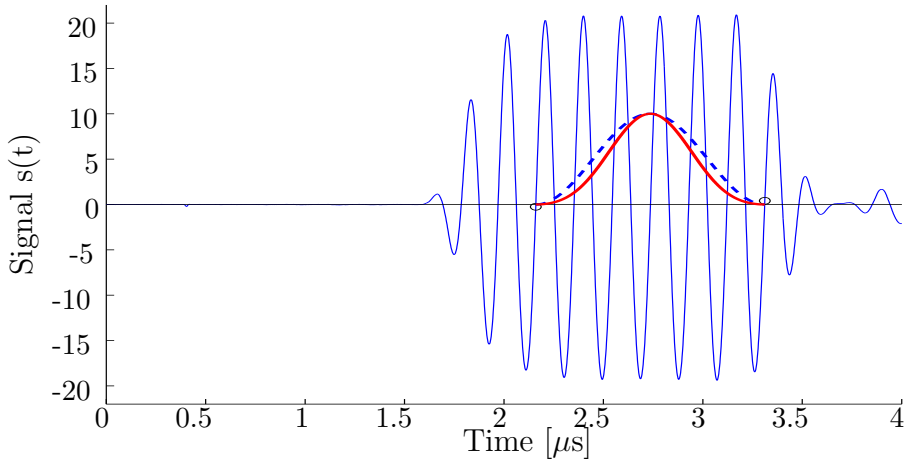

Figure 4.12: Nonlinear measurement, DC-offset subtracted, circles are beginning/end of window (red solid: Blackman window, blue dashed: Hanning window; windows are ploted ten times inflated).

Both, a Hanning and a Blackman window are used for the windowing. The corrected frequency representation in Figure 4.13 shows the absolute amplitudes. The DC part

generated by the nonlinearity of the material cannot be seen because of the frequency properties of the transducer used.

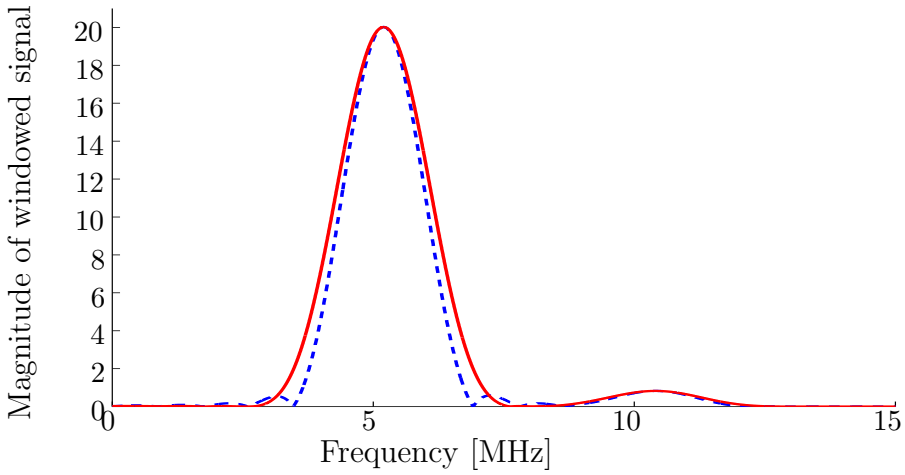

Figure 4.13: Magnitude of windowed signal (red solid: Blackman window, blue dashed: Hanning window).

Using a second signal where the signal to the input transducer is phase-shifted for 180° and adding it up to the first signal results in the second harmonic signal. This signal corrected by the factor 2 is given in Figure 4.14. The red circles indicate again the used range of the signal that is the same used for the windowing.

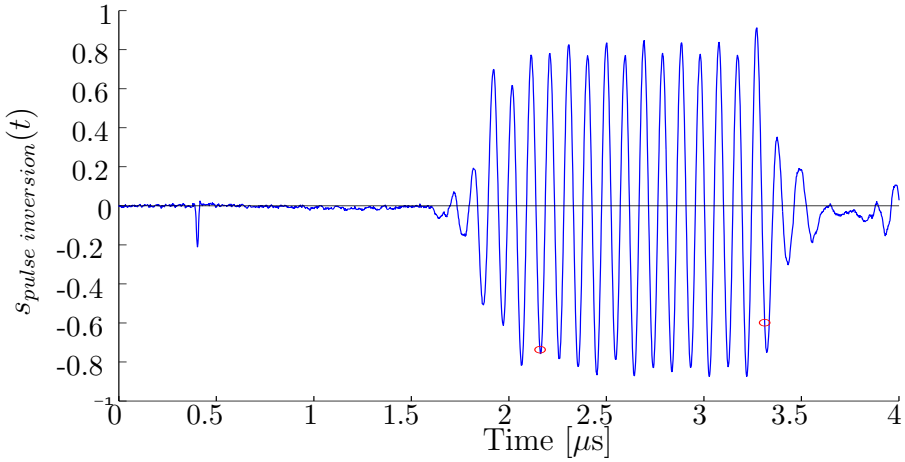

Figure 4.14: Signal after pulse inversion (scaled for factor 2).

Obviously the second harmonic amplitude varys. This effect is due to the transient behavior of the transducers and will vanish for longer signals. To get an absolute value

for the amplitude, the absolute values of all peaks (negative and positive) between the two red circles are averaged.

A comparison between the amplitudes received by windowing and by pulse inversion is given in Table 4.2.

Table 4.2: Comparison between windowing and pulse inversion.

	1st peak		2nd peak		
	f_1	mag_1 (a_1)	f_2	mag_2 (a_2)	mag_2/mag_1^2 (a_2/a_1^2)
Hanning window	5.2 MHz	20.02109	10.415 MHz	0.82651	0.0020619
Blackman window	5.2 MHz	20.01863	10.405 MHz	0.82588	0.0020608
Pulse inversion	-	19.92168	-	0.81888	0.0020633

The Hanning and the Blackman window deliver almost the same value for the first harmonic amplitude. With the pulse inversion only the amplitude of the whole signal instead of the first harmonic can be measured and is therefore less precise. For the second harmonic amplitude, the peaks for both windows are not completely exact at 10.4 MHz but quite close. In Figure 4.15 it can be seen that there is still a little bit of leakage from the first harmonic but only at a very low level. Also the leakage

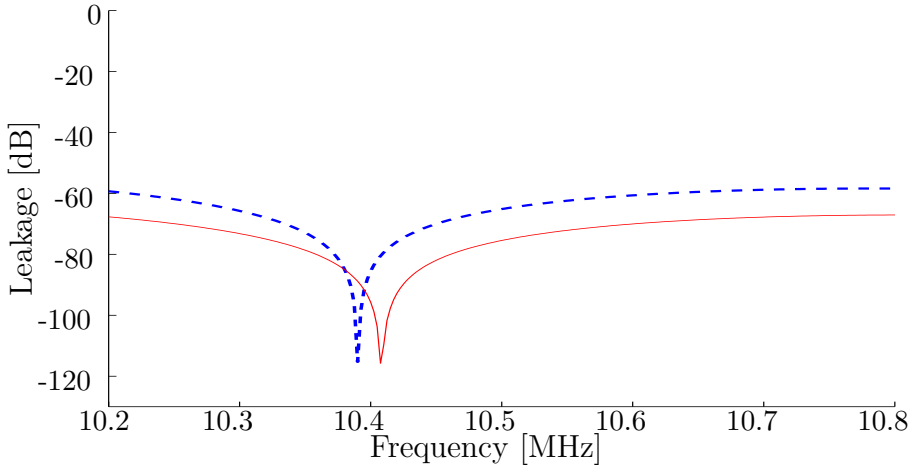

Figure 4.15: Max. Leakage from 5.2 MHz into frequency range around 10.4 MHz in dB of first harmonic amplitude (red solid: Blackman window, blue dashed: Hanning window).

for the Blackman window is smaller than for the Hanning window. The leakage for the Blackman window is less than -80 dB or less than 0.002 in an absolute number. This implies also that the windowing for this signal seems to be slightly more exact than the pulse inversion. However, all values for the ratio of the second harmonic amplitude to the first harmonic amplitude squared in Table 4.2 are all quite close. This value is proportional the the nonlinear parameter β. The results in Table 4.2 are consistent with measurements with lower input signals.

To conclude, both windowing and pulse inversion show enough precision for nonlinear measurements and are therefore appropriate signal processing tools for determining the harmonic amplitudes. Windowing needs only one measurement and delivers one value for each frequency component, pulse inversion requires two measurements and makes an additional averaging necessary to get a value for the second harmonic. Furthermore pulse inversion requires either equipment that can deal very well with exact phase shifts or a correlation between the two signals has to be performed to get an exact phase shift between the two signals. The windowing method allows the determination of even higher harmonics than the second and is therefore less limited than the pulse inversion where only the first and second harmonic amplitude can be determined. Additionally, windowing is slightly more accurate. However for very thin samples, i.e. too short signals, windowing cannot be used any more (minimum window length) and pulse inversion still works.

4.7 Further Signal Processing Methods for Nonlinear Measurements

The final two sections of this chapter deal with two additional signal processing methods that can be used for nonlinear measurements. One eliminates windowing effects and the other allows to determine slightly time varying amplitudes. However they are limited to special cases.

4.7.1 Reconstruction of an Ideal Frequency Representation

Considering that the DFT is a linear operation and that the DFT is the result of a circular convolution of a (rectangular) window with an ideal signal, it is possible to reconstruct an un-windowed ideal frequency representation that does not include any leakage effects and allows therefore an exact determination of the amplitudes of the different frequency components.

4.7.1.1 Definition

An ideal frequency representation is here defined as following.

> An *ideal frequency representation of a finite length signal* is a frequency representation where each frequency component magnitude is represented by a peak whose height depends linearly on its averaged amplitude over the signal length and the signal length itself.

4.7.1.2 Theory

Starting point is the circular convolution

$$X_w[k] = \frac{1}{N} \sum_{l=0}^{N-1} X_{ideal}[l] W[((k-l))_N] \,. \tag{4.17}$$

where the windowed signal $X_w[k]$, the ideal signal $X_{ideal}[k]$ and the window $W[k]$ are in general complex sequences.

Again, only real signals in the time domain are considered and in the signal, the

highest frequency component is smaller than half the sampling frequency, following the Nyquist sampling theorem. $X_{ideal}[k]$ will be zero for most of the k's or frequencies, respectively[4]. It is assumed that the frequency ranges are known that contain the frequency components of the signal x. Therefore the equation for the circular convolution can be reduced to

$$X_w[k] = \frac{1}{N} \sum_{l=l_1,\ldots,l_m} X_{ideal}[l] W[((k-l))_N], \quad m \leq N, \quad m \,\text{even}\,, \tag{4.18}$$

where l are the discrete components of the chosen frequency ranges (symmetric). Considering the symmetry properties of the DFT for real sequences in the time domain given in Equation (4.12), equation (4.18) can be written as

$$X_w[k] = \frac{1}{N}\Big(\quad \sum_{l=l_1,\ldots,l_{m/2}} X[l]_{ideal} W[((k-l))_N] \tag{4.19}$$

$$+ X_{ideal}[l]^{\star} W[((k-(N-(l-1))))_N]\Big)\,. \tag{4.20}$$

To avoid too lengthy terms the following notation is used

$$W^L_{k,l} := \;\; W[((k-l))_N]\,, W^R_{k,l} := \;\; W[((k-(N-(l-1))))_N]\,, \tag{4.21}$$

so that Equation (4.20) becomes

$$X_w[k] = \frac{1}{N}\Big(\quad \sum_{l=l_1,\ldots,l_{m/2}} X[l]_{ideal} W^L_{k,l} + X^{\star}_{ideal}[l] W^R_{k,l}\Big)\,. \tag{4.22}$$

The appearance of $X_{ideal}[k]$ together with its conjugate complex in this system of equations makes it necessary to separate the real and imaginary part of $X_{ideal}[k]$. As a result the size of the system of equations doubles.

The separation for one specific k and l_j in Equation (4.22) is shown as an example. Solving

$$W^L_{k,l_j} X_{ideal}[l_j]\} + W^R_{k,l_j} X^{\star}_{ideal}[l_j] = X_w[k] \tag{4.23}$$

[4]This constraint guarantees the uniqueness of the solution. Otherwise $X_w[k]$ is also a solution for $X_{ideal}[k]$ since windowing a windowed signal with a rectangular window does not change the windowed signal.

with

$$X_{ideal}[l_j] = (Re\{X_{ideal}[l_j]\} + iIm\{X_{ideal}[l_j]\}) \tag{4.24}$$

for the real and imaginary part of $X_{ideal}[l_j]$ leads to the system of equations

$$\mathbf{M_{k,l_j}} \begin{pmatrix} Re\{X_{ideal}[l_j]\} \\ Im\{X_{ideal}[l_j]\} \end{pmatrix} = \begin{pmatrix} Re\{X_w[k]\} \\ Im\{X_w[k]\} \end{pmatrix} \tag{4.25}$$

with

$$\mathbf{M_{k,l_j}} := \begin{pmatrix} Re\{W^L_{k,l_j} + W^R_{k,l_j}\} & Im\{-W^L_{k,l_j} + W^R_{k,l_j}\} \\ Im\{W^L_{k,l_j} + W^R_{k,l_j}\} & Re\{W^L_{k,l_j} - W^R_{k,l_j}\} \end{pmatrix} . \tag{4.26}$$

Finally the whole system of equations in (4.22) can be written in the form

$$\mathbf{M} \begin{pmatrix} Re\{X_{ideal}[l_1]\} \\ Im\{X_{ideal}[l_1]\} \\ \vdots \\ Re\{X_{ideal}[l_{m/2}]\} \\ Im\{X_{ideal}[l_{m/2}]\} \end{pmatrix} = \begin{pmatrix} Re\{X_w[k_1]\} \\ Im\{X_w[k_1]\} \\ \vdots \\ Re\{X_w[k_{m/2}]\} \\ Im\{X_w[k_{m/2}]\} \end{pmatrix} \tag{4.27}$$

where

$$\mathbf{M} = \begin{pmatrix} M_{k_1,l_1} & \dots & M_{k_1,l_{m/2}} \\ \vdots & \vdots & \vdots \\ M_{k_{m/2},l_1} & \dots & M_{k_{m/2},l_{m/2}} \end{pmatrix} . \tag{4.28}$$

The values for l_j are chosen such that the frequency range is covered where the frequency components of the signal are expected. However the values for k can be picked arbitrarily.

4.7.1.3 Examples and Discussion

For the discussion of this method a synthetic signal is used for which the ideal frequency representation is known.

The ideal frequency representation of a sinusoid is given as

$$sin(2\pi f_0/f_s n + \phi) \quad \overset{'\text{ideal}'\mathcal{DFT}}{\leftrightarrow} \quad \frac{N}{2}\sum_{k=0}^{N-1}[e^{i(\phi-\pi/2)}\delta(k-k_0) + e^{-i(\phi-\pi/2)}\delta(k-(N+2-k_0))]\,, \tag{4.29}$$

where f_0, f_s and N are such that k_0 is the discrete index for the frequency f_0. Both, the origin from the continuous Fourier transform as well as the discrete nature without windowing effects can be seen.

The ideal frequency representation of a sinusoid is justified by doing a circular convolution of the ideal frequency representation with a rectangular window, e.g. following Equation (4.11). The real and imaginary part of this circular convolution coincides with the real and imaginary part of the DFT of the sinusoid.

As an example the following signal is used,

$$s(t) = 1 * sin(2\pi\, 5\,\text{MHz} * t + \pi/4) + 0.01 * sin(2\pi\, 10\,\text{MHz} * t + \pi/8)\,. \tag{4.30}$$

One and five 5 MHz cycles are considered, for the discretization a sampling rate of 500 MHz is used and to the discrete time signal zeros are appended for a total of N=2000 discrete points. The additional phase shifts in the sinusoids are included to demonstrate the general validity of this method. For the discussion of the reconstructed ideal frequency representation the length of the ranges where the frequencies are expected (l_j) are varied in length what makes it also necessary to adapt the number of values for k.

In the following Tables (Table 4.3 to 4.8) the reconstructed signal is compared with the ideal signal.

Table 4.3: Reconstruction of ideal frequency representation
(1 cycle, $k = [6, 15, 20, 25, 26, 27]$).

l_j	ideal frequency representation		ideal frequency representation (reconstructed)	
20	0	$0i$	-0.00258417	$+0.01336840i$
21	35.35533905	$-35.35533905i$	35.35635220	$-35.38373704i$
22	0	$0i$	0.00178971	$+0.01488964i$
40	0	$0i$	-0.00099293	$+0.00429448i$
41	0.19134171	$-0.46193976i$	0.19186431	$-0.46918671i$
42	0	$0i$	0.00025153	$+0.00301503i$

Table 4.4: Reconstruction of ideal frequency representation
(5 cycles, $k = [6, 15, 20, 25, 26, 27]$).

l_j	ideal frequency representation		ideal frequency representation (reconstructed)	
20	0	$0i$	0.00000000	$+0.00000000i$
21	176.77669529	$-176.77669529i$	176.77669529	$-176.77669529i$
22	0	$0i$	0.00000000	$-0.00000000i$
40	0	$0i$	0.00000000	$-0.00000000i$
41	0.95670858	$-2.30969883i$	0.95670858	$-2.30969883i$
42	0	$0i$	-0.00000000	$-0.00000000i$

Table 4.5: Reconstruction of ideal frequency representation
(1 cycle, $k = [6, 15, 20, 25, 26, 27, 41, 50]$).

l_j	ideal frequency representation		ideal frequency representation (reconstructed)	
20	0	$0i$	-5.53117077	$+2.62803145i$
21	35.35533905	$-35.35533905i$	51.99136803	$-46.26371607i$
22	0	$0i$	-16.42709987	$+14.37390223i$
23	0	$0i$	5.29001526	$-6.12953400i$
40	0	$0i$	2.07159904	$-0.49415698i$
41	0.19134171	$-0.46193976i$	-4.33813415	$+1.38499154i$
42	0	$0i$	3.25292678	$-1.95226861i$
43	0	$0i$	-0.76282343	$+0.63501759i$

Table 4.6: Reconstruction of ideal frequency representation
(5 cycles, $k = [6, 15, 20, 25, 26, 27, 41, 50]$).

l_j	ideal frequency representation		ideal frequency representation (reconstructed)	
20	0	$+0i$	-0.00000000	-0.00000000i
21	176.77669529	-176.77669529i	176.77669529	-176.77669529i
22	0	$+0i$	-0.00000000	+0.00000000i
23	0	$+0i$	-0.00000000	-0.00000000i
40	0	$+0i$	0.00000000	+0.00000000i
41	0.95670858	-2.30969883i	0.95670858	-2.30969883i
42	0	$+ 0i$	0.00000000	-0.00000000i
43	0	$+ 0i$	-0.00000000	+0.00000000i

Table 4.7: Reconstruction of ideal frequency representation
(1 cycle, $k = [6, 15, 20, 25, 26, 27, 41, 50, 70, 90]$).

l_j	ideal frequency representation		ideal frequency representation (reconstructed)	
19	0	$+0i$	-5.7271494585	-.1554127063i
20	0	$+0i$	16.3495701388	11.3390828779i
21	35.3553390593	-35.3553390593i	25.5785280887	-47.4755186633i
22	0	$+0i$	-7.1868815163	8.0499244276i
23	0	$+0i$	6.3778189693	-3.2636905944i
39	0	$+0i$	14.4688714668	11.6058018149i
40	0	$+0i$	-47.8849073580	-28.2399661958i
41	0.1913417161	-0.4619397662i	58.7750491767	23.5798154046i
42	0	$+ 0i$	-31.4805051473	-7.8975235198i
43	0	$+ 0i$	6.2762864074	0.6423259405i

Table 4.8: Reconstruction of ideal frequency representation
(5 cycle, $k = [6, 15, 20, 25, 26, 27, 41, 50, 70, 90]$).

l_j	ideal frequency representation		ideal frequency representation (reconstructed)	
19	0	$+0i$	0.00000000	$0.00000000i$
20	0	$+0i$	-0.00000000	$0.00000000i$
21	176.77669529	$-176.77669529i$	176.77669529	$-176.77669529i$
22	0	$+0i$	0.00000000	$0.00000000i$
23	0	$+0i$	-0.00000000	$-0.00000000i$
39	0	$+0i$	-0.00000000	$-0.00000000i$
40	0	$+0i$	0.00000000	$-0.00000000i$
41	0.95670858	$-2.30969883i$	0.95670858	$-2.30969883i$
42	0	$+ 0i$	-0.00000000	$-0.00000000i$
43	0	$+ 0i$	0.00000000	$0.00000000i$

Table 4.9: Condition of matrix $\mathbf{M}$.

cycles	6pts, A	8pts, B	10pts, C
1	2.35×10^{13}	2.14×10^{16}	8.71×10^{16}
5	1.14×10^{4}	1.54×10^{4}	7.06×10^{4}

A: $k = [6, 15, 20, 25, 26, 27]$, $l_j = [20, 21, 22, 40, 41, 42]$
B: $k = [6, 15, 20, 25, 26, 27, 41, 50]$, $l_j = [20, 21, 22, 23, 40, 41, 42, 43]$
C: $k = [6, 15, 20, 25, 26, 27, 41, 50, 70, 90]$, $l_j = [19, 20, 21, 22, 23, 39, 40, 41, 42, 43]$

In some cases the reconstructed ideal frequency representation coincides extremely well (e.g. Tables 4.4, 4.6 and 4.8) in other cases (Tables 4.5 and 4.7) the correspondence is very poor. The different results are only due to roundoff errors while solving the system of equations numerically.

A useful measure for the loss of precision due to roundoff errors is given in the condition number (2-norm) of the matrix $\mathbf{M}$ [32]. Usually the rule is that the exponent $log10(condition(\mathbf{M}))$ of the condition number indicates the number of decimal places that can be lost due to roundoff errors. The condition number of the matrix $\mathbf{M}$ for the different reconstructions is given in Table 4.9. Considering that the standard double precision numbers used in Matlab[5] have about 16 decimal digits of accuracy the different results for the ideal frequency representation become obvious.

The condition number for $\mathbf{M}$ depends on the values for k, the size of the matrix (depends on the length of the frequecy ranges in l_j) and the signal length. Different k's change the entries in $\mathbf{M}$, an increased size of $\mathbf{M}$ increases the probability that the matrix is ill-conditioned and the length of the signal scales its entry values.

The need of a discrete frequency sample at the exact frequency of each signal component as well as the aspect of ill-conditioning for numerical solutions limits this method and makes it difficult to apply it to a real signal.

[5]For all calculations in this section Matlab Version 7.0.1 (R14) is used.

4.7.2 Short-Time Fourier Transformation (STFT)-based Reconstruction of Time-dependent Harmonic Amplitudes

This section deals with a proposed method to reconstruct slowly time-varying amplitudes of harmonics based on the Short-Time Fourier transform (STFT). The main challenge again is the extremely different range of the amplitudes of the the harmonic frequencies.

First, the STFT is described, then it is shown how the understanding of windowing helps to choose a window in order to reconsctruct the amplitude by applying it to a synthetic signal.

4.7.2.1 Short-Time Fourier Transform (STFT)

The STFT is a time-frequency representation of signal. For a continuous infinite-length signal $x(t)$ it is given by

$$F_x(t,\nu;w) = \int_{-\infty}^{\infty} x(u)w^{\star}(u-t)e^{-i2\pi\nu u}du\,, \tag{4.31}$$

where w is a window and t and ν are the time-frequency coordinates for which the STFT is evaluated.

A graphical interpretation of the STFT in the time domain is given in Figure 4.16. The window w is positioned at a specific time t so that only the part of the time signal around t is used for the FFT that in performed on the windowed signal, as described in equation (4.31). Doing this for every time t results in a time-frequency representation.

The STFT may also be expressed in terms of signal and window spectra (proof given in appendix B.2)

$$F_x(t,\nu;h) = \frac{1}{2\pi}\int_{-\infty}^{\infty} X(\xi)W(\xi-\nu)e^{i2\pi(\xi-\nu)t}d\xi \tag{4.32}$$

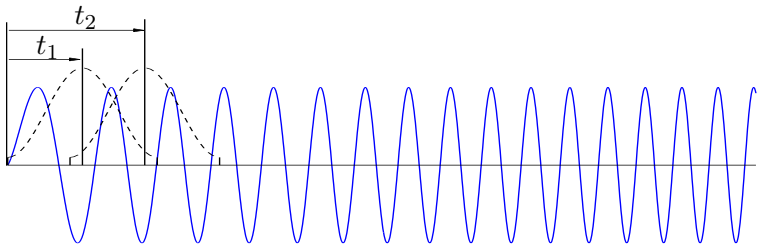

Figure 4.16: Principle of the STFT in the time domain (dashed line: window centered at two different times t_1 and t_2).

where X and W are respectively the Fourier transforms of x and w.

This expression opens up an interpretation for the STFT in the frequency domain, any frequency variation of the STFT for any fixed time can be interpreted as a smoothed version of the Fourier transform of the underlying signal (Figure 4.17). For the calcu-

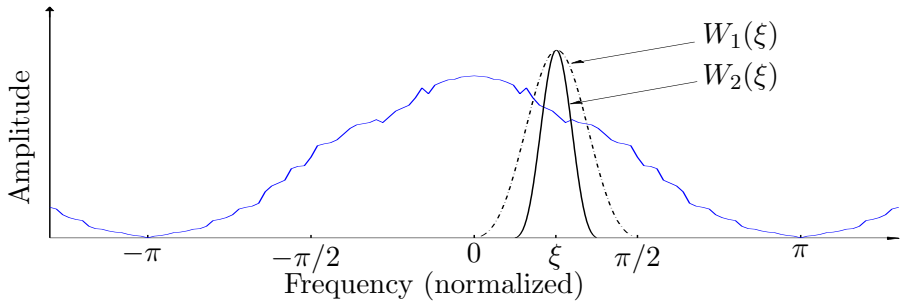

Figure 4.17: Window as smoothing function in the frequency domain ($W_1(\xi)$ wideband, $W_2(\xi)$ narrowband window).

lation of the STFT at a specific frequency ν the window is centered at this frequency, multiplied with the signal $X(\xi)$ and the exponential term and integrated over the complete (positive and negative) frequency range as described in equation (4.32). The narrower the the bandwidth of the window $W(\xi)$, the better the frequency resolution of the STFT, but also the longer the window and therefore the worse the time resolution. One extreme case is that the window $W(\xi)$ is just an impulse with perfect frequency resolution, but no time resolution. The choice of the window follows similar rules as in section 4.3. However, the position of the zeros in the frequency domain plays a crucial role.

4.7.2.2 Reconstruction of the amplitude of different signal components

Taking the absolute value of equation (4.32) delivers

$$|F_x(t,\nu;h)| = |\frac{1}{2\pi}\int_{-\infty}^{\infty} X(\xi)W(\xi-\nu)e^{i2\pi(\xi-\nu)t}d\xi| \tag{4.33}$$

$$= |\frac{1}{2\pi}\int_{-\infty}^{\infty} X(\xi)W(\xi-\nu)e^{i2\pi\xi t}d\xi||e^{-i2\pi\nu t}| \tag{4.34}$$

$$= |\frac{1}{2\pi}\int_{-\infty}^{\infty} X(\xi)W(\xi-\nu)e^{i2\pi\xi t}d\xi| \tag{4.35}$$

The inner term $X(\xi)W(\xi-\nu)$ in equation (4.35) is nothing other than filtering the signal $X(\xi)$ with the frequency shifted window $W(\xi-\nu)$. On the filtered signal is an inverse Fourier transform applied and the absolute value is taken. Considering this and assuming that the window $W(\xi-\nu)$ is designed in a way that it filters out the other frequency components when centered at a harmonic frequency ν then we can perfectly reconstruct its slowly time-varying amplitude. This method is limited to slowly time-varying amplitudes, otherwise the variation of the amplitude will add additional frequency components that might leak into the harmonic frequencies when applying the window in the STFT and might worsen the reconstruction.

4.7.2.3 The Discrete STFT

The discrete STFT is realized using the algorithm from the Time-Frequency Toolbox (TFTB) for Matlab. The algorithm is basically a discrete version of equation (4.31). It is restricted to windows with an odd length. Due to the finite length of the signal the output at the beginning and end of the signal (about half the window length respectively) cannot be used. Of course the output amplitude has to be corrected for the used window.

4.7.2.4 Example

Given is a synthetic signal $s(t)$ consisting of three harmonically related components which are given as

$$s_1(t) = a_1 \sin(2\pi f_1 t), \quad f_1 = 5\text{MHz}, \quad a_1(t) = 200 \tag{4.36}$$

$$s_2(t) = a_2 \sin(2\pi f_2 t), \quad f_2 = 10\text{MHz}, \quad a_2(t) = 2/(1 + e^{-t10^6}) \tag{4.37}$$

$$s_3(t) = a_3 \sin(2\pi f_3 t), \quad f_3 = 15\text{MHz}, \quad a_3(t) = t10^4\,, \tag{4.38}$$

The complete signal is the sum of the components,

$$s(t) = s_1(t) + s_2(t) + s_3(t)\,. \tag{4.39}$$

The signal is sampled with a frequency of $f_s = 500\text{MHz}$ and 1000 samples are used, starting with $t = 0$.

The goal is to reconstruct the amplitudes $a_1(t)$, $a_2(t)$ and $a_3(t)$ over time. Note the extreme differences in the amplitudes, $a_1(t) \approx a_2(t) \times 10^2 \approx a_3(t) \times 10^4$.

For the STFT, an appropriate Blackman window of length 301 is used as depicted in Figure 4.18. This window has zeros at multiples of 5 MHz. Therefore there is no leakage from one harmonic into the other. Even when the frequency is not exactly 5 MHz there is already an attenuation of -80 dB (Figure 18(b)). Therefore the other harmonics are filtered out when evaluating the amplitude for a harmonic frequency.

The results of the STFT-based reconstruction of the amplitudes $a_1(t)$ to $a_3(t)$ are shown in the Figures 19(a) to 19(c). As mentioned earlier, the reconstructed amplitudes are not valid for the whole time range of 1000 samples. With a window length of 301 the first and last 150 samples cannot be used. In the range between about 150 to 850 time samples the reconstructed amplitudes are quite close to the real amplitudes. Only very small deflections can be observed.

The reconstructed amplitudes are not influenced by any phase shift in one of the signal components since the absolute value of the STFT is used for the reconstruction.

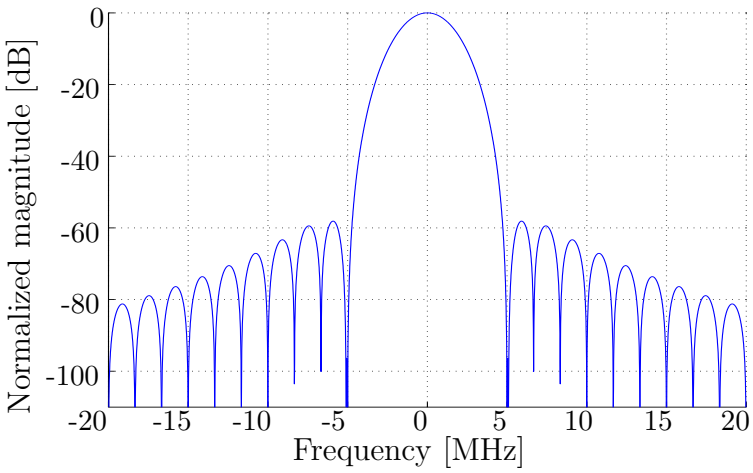

(a) Blackman window (-20 to +20 MHz)

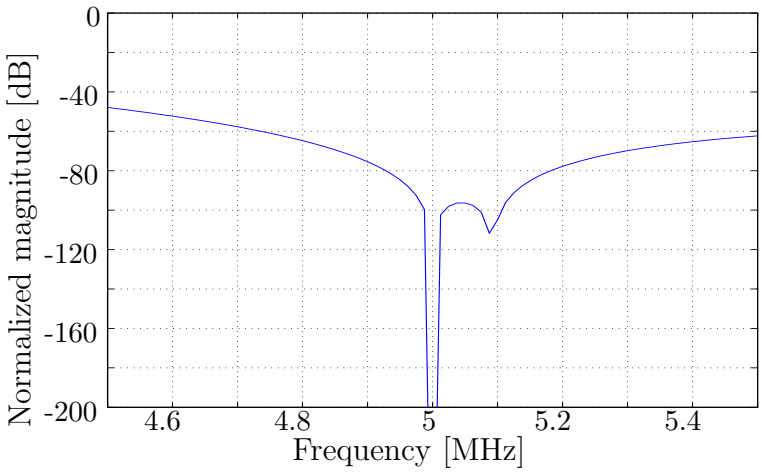

(b) Blackman window (4.5 to 5.5 MHz)

Figure 4.18: Blackman window (length 301, f_s=500 MHz) for a STFT-based reconstruction of the harmonics (f=5, 10, 15 MHz).

In Figure 4.20 a part of the STFT of the signal corrected for the amplitude change due to the window is depicted. Figures 19(a) to 19(c) are just slices of the STFT in Figure 4.20 at specific frequencies. In Figure 4.20 we can clearly see the effects of the right choice of the window. As described before at 10 and 15 MHz there is no leakage from the other frequency components but at the frequencies in between.

The window in this example is chosen such that the zeros are as close as possible at the harmonic frequencies and such that there is a high attenuation. The time resolution is less important in this example. However in other examples it might be

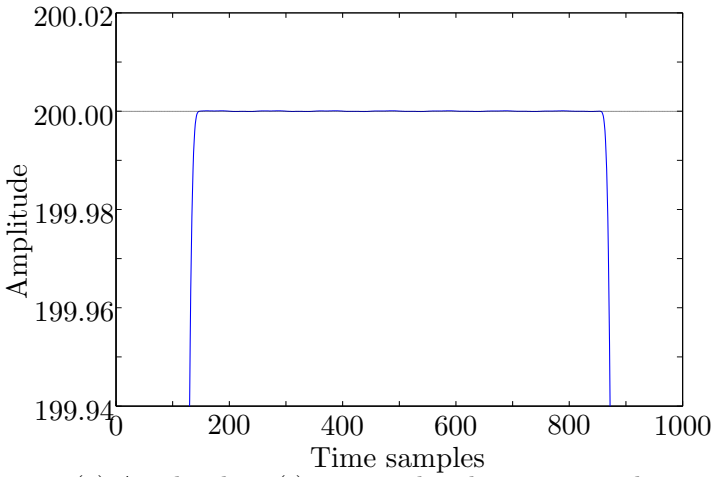

(a) Amplitude $a_1(t)$, expected and reconstructed.

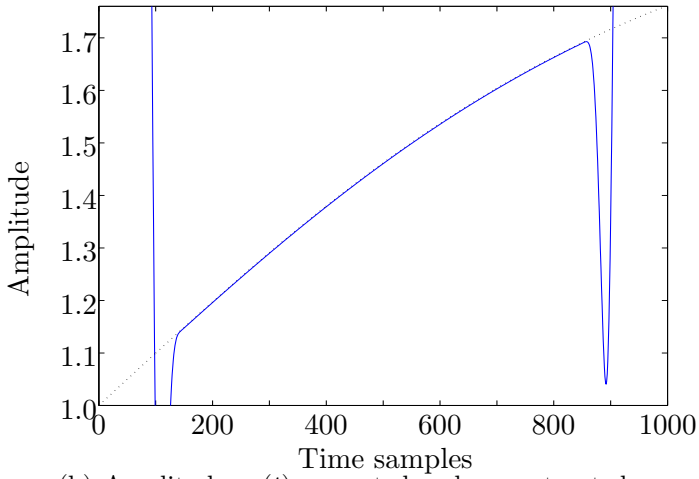

(b) Amplitude $a_2(t)$, expected and reconstructed.

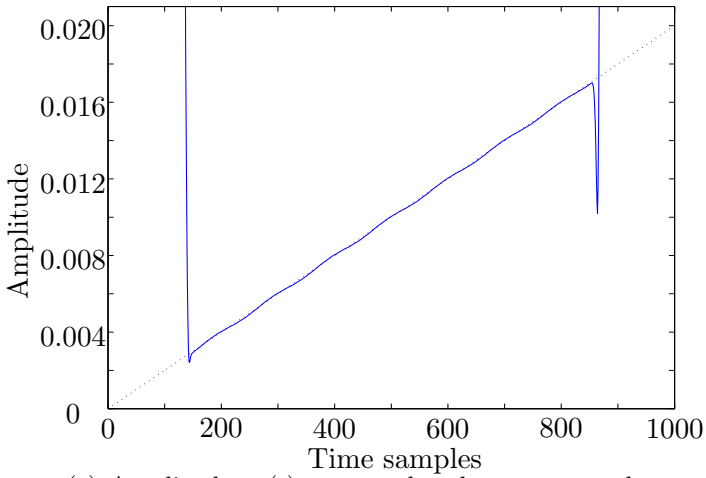

(c) Amplitude $a_3(t)$, expected and reconstructed.

Figure 4.19: STFT-based reconstruction of slightly time-varying harmonic amplitudes.

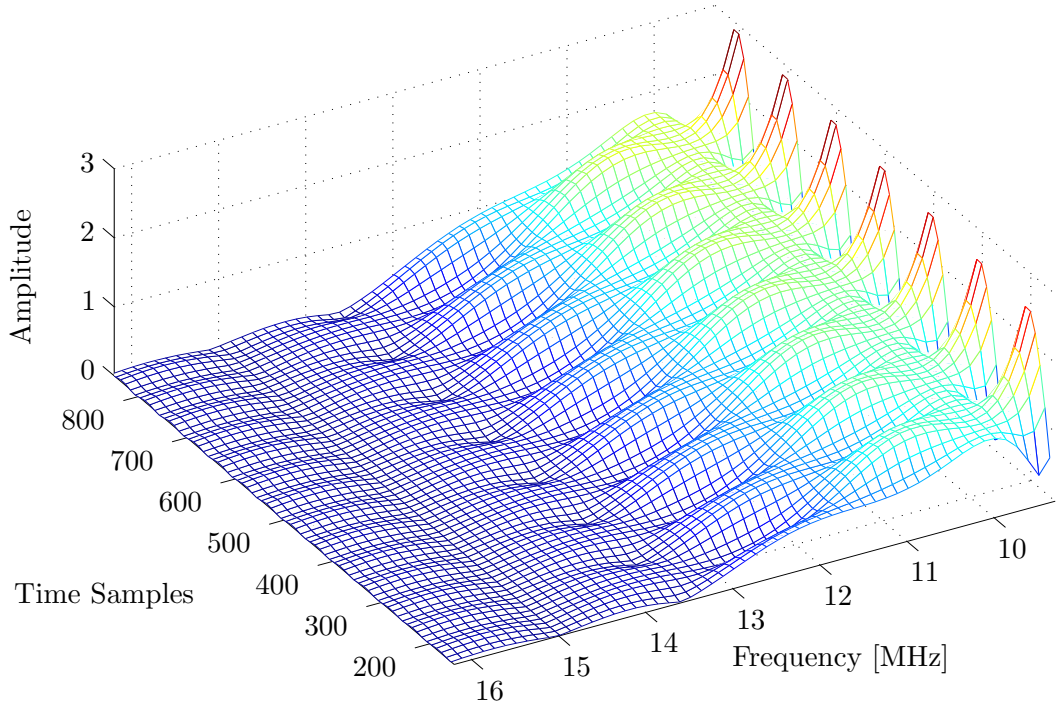

Figure 4.20: STFT of signal $s(t)$ with normalized Blackman window of length 301.

necessary to find a compromise between time resolution, i.e. window length, and attenuation.

As demonstrated, the method works well for the reconstruction of slowly time varying harmonic amplitudes. It is based on the ideas and the understanding of windowing. Crucial is the compromise between the window length, the position of the zeros and attenuation. The advantage of this approach is that the only thing that has to be known about the harmonic signal is the frequency and that the amplitude is slowly varying in contrast to other approaches where a model for the signal is required, e.g. in [29].

CHAPTER V

RAYLEIGH WAVES FOR NONLINEAR MEASUREMENTS

Rayleigh waves are a specific type of elastic wave that travels on the surface of a body without propagating into it. Therefore Rayleigh waves are very efficient in the detection of fatigue damage initiated and concentrated at the surface.
In this chapter the theory of linear Rayleigh waves is shortly described [1, 18]. Based on the linear theory a model for the nonlinear case [33] is shown and is used for introducing a nonlinear parameter for surface waves.

5.1 Theory of Linear Rayleigh Waves

For isotropic linear elastic material the equation of motion (2.12) can be written as

$$\frac{\partial^2 u}{\partial t^2} - c_{\mathrm{L/T}}^2 \Delta u = 0\,, \tag{5.1}$$

where u is any component of the displacement vectors $\mathbf{u}_{\mathrm{L}}$ or $\mathbf{u}_{\mathrm{T}}$ of the longitudinal or transversal wave respectively with

$$\mathbf{u} = \mathbf{u}_{\mathrm{L}} + \mathbf{u}_{\mathrm{T}}, \quad \operatorname{div} \mathbf{u}_{\mathrm{T}} = 0 \quad \text{and} \quad \operatorname{curl} \mathbf{u}_{\mathrm{L}} = 0\,. \tag{5.2}$$

The scalar $c_{\mathrm{L/T}}$ is the corresponding velocity c_{L} or c_{T} that are calculated according to Equation (2.11).

Here only the two-dimensional case of a plane monochromatic wave propagating along the infinite free surface of an elastic half-space, as shown in Figure 5.1, is considered. The medium is in $z < 0$.

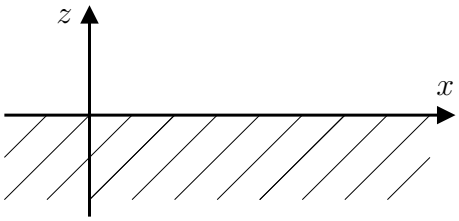

Figure 5.1: Coordinates for Rayleigh waves.

The solution of the equations of motion above (5.1) has the form

$$u_{\mathrm{L/T}} = \mathrm{constant}_{\mathrm{L/T}} \times e^{i(kx-\omega t)} e^{\kappa_{\mathrm{L/T}} z}\,, \tag{5.3}$$

where

$$\kappa_{\mathrm{L/T}} = \sqrt{k^2 - \omega^2/c_{\mathrm{L/T}}^2}\,, \tag{5.4}$$

where $\kappa_{\mathrm{L/T}}$ determines the rate of the exponential decay of the displacement with distance from the surface, a characteristic of Rayleigh waves.

The relation between the wave number k, the circular frequency ω and the phase velocity of Rayleigh waves, c_{R}, is given by

$$k = \frac{\omega}{c_{\mathrm{R}}}\,. \tag{5.5}$$

With the boundary condition of a free surface at $z = 0$ (traction is zero), Equation (5.3) and Equation (5.5) follows, after some calculations, the well-known characteristic equation for the phase velocity of Rayleigh waves,

$$\left(2 - \frac{c_{\mathrm{R}}^2}{c_{\mathrm{T}}^2}\right)^2 - 4\left(1 - \frac{c_{\mathrm{R}}^2}{c_{\mathrm{L}}^2}\right)^{\frac{1}{2}}\left(1 - \frac{c_{\mathrm{R}}^2}{c_{\mathrm{T}}^2}\right)^{\frac{1}{2}} = 0\,. \tag{5.6}$$

For the phase velocity of Rayleigh waves an approximation is also given using Poisson's ratio ν_P [1],

$$c_{\mathrm{R}} \approx \frac{0.862 + 1.14\nu_P}{1 + \nu_P} c_{\mathrm{T}}\,. \tag{5.7}$$

Consequently the propagation speed of Rayleigh waves is independent of the frequency (nondispersive) in a non-absorbing homogeneous medium.

It is convenient to introduce a nondimensional constant for the ratio between the velocity of the surface waves according to

$$\xi = c_{\mathrm{R}}/c_{\mathrm{T}} < 1\,. \tag{5.8}$$

Finally the particle displacements in the x- and z-direction yield

$$u_x(x,z,t) = i\,b\,\left[\xi_t\, e^{(\xi_t\, k\, z)} + \eta\, e^{(\xi_l\, k\, z)}\right] e^{i(k\,x-\omega\,t)} \tag{5.9}$$

$$u_z(x,z,t) = b\,\left[e^{(\xi_t\, k\, z)} + \eta\, \xi_l e^{(\xi_l\, k\, z)}\right] e^{i(k\,x-\omega\,t)} \tag{5.10}$$

with

$$\xi_t = \sqrt{1-\xi^2} \tag{5.11}$$

$$\xi_l = \sqrt{1-\xi^2 c_{\mathrm{T}}^2/c_{\mathrm{L}}^2} \tag{5.12}$$

$$\eta = -2\frac{(1-\xi^2)^{1/2}}{(2-\xi^2)} \tag{5.13}$$

where ξ_l characterizes the decay rate of the longitudinal wave part, ξ_t the decay rate of the transverse part and η is the ratio of both. The scalar b is a simple amplitude factor. In the displacement equations above it can be seen again that the displacement in each direction has contributions from the longitudinal and transversal waves. Note that the material is in $z \leq 0$.

The lack of velocity dispersion is a major advantage of surface waves for nonlinear application since it allows nonlinearity to accumulate with distance [25]. A further advantage is that the energy is mainly concentrated near the surface where fatigue damage is usually accumulated.

The equations for linear Rayleigh waves are also the starting point for the nonlinear case. More details about Rayleigh waves in a linear elastic material and the exact calculation of the equations above can be found in [18, 1].

5.2 A Model for Rayleigh Waves in Nonlinear Materials

As seen earlier, the solution for longitudinal or bulk waves in nonlinear isotropic material is obtained based on approximation techniques. Here in this chapter a model for Rayleigh waves in nonlinear isotropic material, suggested by Zabolotskaya [33] and Shull et al. [26], is used.

5.2.1 Model

The model is based on the linear solution for Rayleigh waves combined with Hamiltonian equations of multi modal systems in the analytical dynamics under the assumption that there are no attenuation effects or other forms of energy losses. This approach can also be found in [2].

Since the propagation speed of Rayleigh waves is independent of the frequency, all harmonics generated due to the nonlinearity have the same velocities and interact efficiently.

The starting point are the displacement equations (5.9) and (5.10) for Rayleigh waves in linear elastic material. All equations in Section 5.1 are valid for this section as long it is not indicated otherwise. Again the wave propagates in x-direction. The total displacement in one direction is modeled as a superposition of the particle displacements of the harmonics in this direction,

$$u_x(x,z,t) = \frac{1}{2}\sum_{n=-\infty}^{+\infty} a_n(t)u_{x,n}(z)exp(in(k_0x)) \quad \text{and} \tag{5.14}$$

$$u_z(x,z,t) = \frac{1}{2}\sum_{n=-\infty}^{+\infty} a_n(t)u_{z,n}(z)exp(in(k_0x))\,, \tag{5.15}$$

where

$$u_{x,n}(z) = i\frac{n}{|n|}\left[\xi_t exp(|n|\xi_t k_0 z) + \eta exp(|n|\xi_l k_0 z)\right]\,, \tag{5.16}$$

$$u_{z,n}(z) = exp(|n|\xi_t k_0 z) + \eta\xi_l exp(|n|\xi_l k_0 z)\,, \tag{5.17}$$

and

$$a_n(t) = b_n exp(-i|n|\omega_0 t) + b^{\star}_{-n} exp(i|n|\omega_0 t)\,. \tag{5.18}$$

The index n indicates the order of the harmonics and takes the values ± 1, ± 2, ... The sign in n comes from the wave vector $\mathbf{k_n} = n\mathbf{k_0}$ of the different harmonics. Note that $\mathbf{k_0}$ is in x-direction and that $|\mathbf{k_0}| = k_0$ is the wavenumber of the first harmonic (n=1) with $k_0 = \omega_0/c_{\mathrm{R}}$. The amplitude of the different modes, $a_n(t)$, finally takes into account that a wave can propagate into different directions. It is assumed that b_n is a slowly varying amplitude. This allows for the approximation

$$\dot{a}_n(t) = -i|n|\omega \left[b_n exp(-i|n|\omega_0 t) + b^{\star}_{-n} exp(i|n|\omega_0 t) \right]\,. \tag{5.19}$$

In the next step the Hamiltonian of this system is constructed. The Hamiltonian is the sum of the kinetic energy and the elastic energy potential,

$$H = \int \frac{\rho}{2}(\dot{u}_x^2 + \dot{u}_z^2) dx dz + \int E dx dz\,, \tag{5.20}$$

where E is the strain energy function given in Equation (2.17).

Some manipulations as well as the exploitation of symmetry properties result in a partial differential equation for the spectral amplitudes v_n. The assumption of steady-state leads to the following system of first order differential equations

$$\frac{dv_n}{dx} = \frac{n^2}{v_0 \bar{x}} \left(2 \sum_{m=n+1}^{\infty} R_{m,n-m} v_m v^{\star}_{m-n} - \sum_{m=1}^{n-1} R_{m,n-m} v_m v_{n-m} \right)\,, \tag{5.21}$$

where v_n $(n = 1, 2, \dots)$ are the spectral velocity amplitudes, v_0 is the velocity amplitude at the source and $\bar{x} = 2\rho c_{\mathrm{R}}^3 \zeta/(\mu k_0 v_0)$ a characteristic length scale with $\zeta = \xi_t + \xi_t^{-1} + \eta^2 \left(\xi_l + \xi_l^{-1}\right) + 4\eta$. The coupling matrix $R_{m,l}$ for the interaction between the different spectral velocity amplitudes v_n depends solemnly on the material properties and the velocity ratios that are also material dependent.

The matrix $R_{m,l}$ is given as

$$R_{m,l} = \frac{\alpha'}{|n|\xi_l + |l|\xi_t + |m|\xi_t} + \frac{\alpha'}{|n|\xi_t + |l|\xi_t + |m|\xi_l} \tag{5.22}$$

$$+\frac{\alpha'}{|n|\xi_t + |l|\xi_l + |m|\xi_t} + \frac{\beta'}{|n|\xi_t + |l|\xi_l + |m|\xi_l} \tag{5.23}$$

$$+\frac{\beta'}{|n|\xi_l + |l|\xi_t + |m|\xi_l} + \frac{\beta'}{|n|\xi_l + |l|\xi_l + |m|\xi_t} \tag{5.24}$$

$$+\frac{3\gamma'}{|n|\xi_l + |l|\xi_l + |m|\xi_l} \tag{5.25}$$

where $n = m + l$ and

$$\alpha' = \alpha + \delta \tag{5.26}$$

$$\beta' = \beta \tag{5.27}$$

$$\gamma' = \gamma + \frac{1}{3}\left[\nu + 2\xi_l(\epsilon - 2\delta)/(\xi_t + \xi_l)\right] \tag{5.28}$$

and

$$\alpha = \eta(7\mu/3 + A + 2B + K)(1 - \xi_l^2)\xi_t^2/\mu \tag{5.29}$$

$$\beta = \eta^2(7\mu/3 + A + 2B + K)(1 - \xi_l^4)\xi_t/\mu \tag{5.30}$$

$$\gamma = \eta^3[(\mu + A/3)(1 + \xi_l^2 + \xi_l^4) + (B + K/2 - \mu/3)(1 + \xi_l^4) \tag{5.31}$$

$$+C(1 - \xi_l^2)^2/3](1 - \xi_l^2)/\mu \tag{5.32}$$

$$\delta = \eta[(\mu + A/4)(1 + \xi_t^2 + \xi_t^4) + A\xi_t^2/4 + B(1 + \xi_t^2)^2/2 \tag{5.33}$$

$$+(K/2 - \mu/3)(1 + \xi_t^4)](1 - \xi_l^2)/\mu \tag{5.34}$$

$$\epsilon = \eta^2(7\mu/3 + A + 2B + K)(1 + \xi_t^2)(1 - \xi_l^2)\xi_l/\mu \tag{5.35}$$

$$\nu = \eta^3(7\mu/3 + A + 2B + K)(1 - \xi_l^2)\xi_l^2/\mu\,. \tag{5.36}$$

The solution of this differential equation is then used to calculate the particle velocities of the Rayleigh wave in x- and z-direction as following,

$$v_x(x, z, t) = \frac{1}{2}\sum_{n=-\infty}^{\infty} v_n(x) u_{x,n}(z) e^{in(k_0 x - \omega t)} \quad \text{and} \tag{5.37}$$

$$v_z(x, z, t) = \frac{1}{2}\sum_{n=-\infty}^{\infty} v_n(x) u_{z,n}(z) e^{in(k_0 x - \omega t)}\,. \tag{5.38}$$

Since the numerical integration of the differential Equation 5.21 becomes numerically instable a damping term α_n is added to the left-hand side. α_n is the small signal attenuation coefficient at frequency $n\omega_0$ and is introduced to be proportional to the square of the frequency with $\alpha_n = constant \times n^2$. The differential Equation 5.21 becomes then

$$\frac{dv_n}{dx} + \alpha_n v_n = \frac{n^2}{v_0 \bar{x}} \left(2 \sum_{m=n+1}^{\infty} R_{m,n-m} v_m v^{\star}_{m-n} - \sum_{m=1}^{n-1} R_{m,n-m} v_m v_{n-m} \right) . \qquad (5.39)$$

Note that the spectral amplitude for real signals satisfies the relation $v^{\star}_n = v_{-n}$.

5.2.2 Discussion

The main interest in [33, 26] is to see how harmonics are generated by Rayleigh waves in a nonlinear isotropic material and to determine the shape of the resulting wave forms. In this research, the interest lies in how the generated harmonics can be used to track changes in the material.

For this and the following simulations, constants for steel are used. The values given in Table 5.1 are either from [33] or are reasonable assumptions for steel.

Table 5.1: Constants used for the simulation (steel).

Elastic constants	A	-0.76×10^{12}	N/m^2
	B	-0.25×10^{12}	N/m^2
	C	-0.09×10^{12}	N/m^2
	K	0.145×10^{12}	N/m^2
	μ	0.0787×10^{12}	N/m^2
Density	ρ	7800	kg/m^3
Circular frequency	ω	$5/(2\pi)$	rad MHz
Initial velocity amplitude (at source)	v_0	1	m/s^2
Small signal attenuation coefficient	α_n	$0.01/(v_0\bar{x}) \times n^2$	m/s^2

In Figure 5.2, the numerical solution for Equation (5.39), using a standard Runge-Kutta integration routine and the constants above, is shown. The first (fundamental)

harmonic velocity amplitude to the fourth harmonic velocity amplitude of the 128 harmonics considered in the simulation are shown. They are plotted over the distance that is normalized by $\bar{x}$. The distance $\bar{x}$ is with the values above (Table 5.1) is approximately 3.53 m.

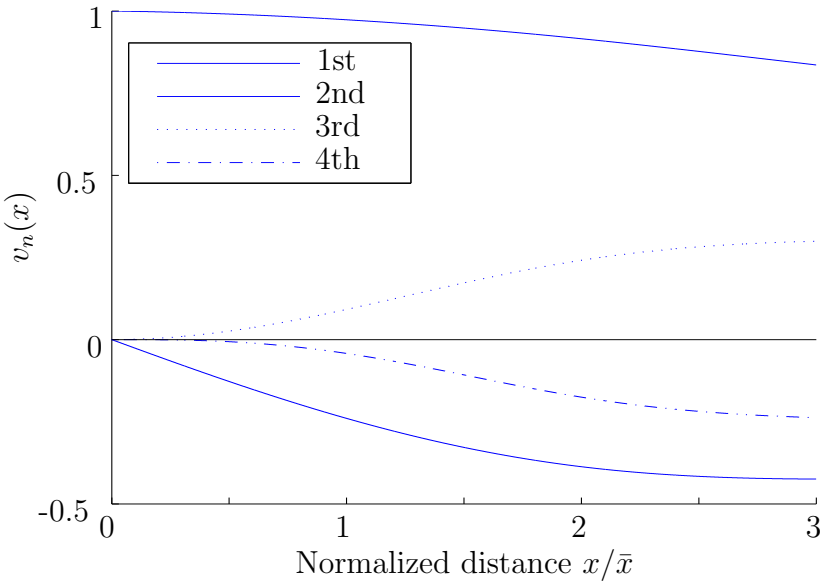

Figure 5.2: Spectral velocity amplitudes (1st to 4th harmonic), calculated with 128 harmonics, constants as in Table 5.1.

The first harmonic starts at $x/\bar{x} = 0$ with the initial value v_0, all other harmonics are zero. Slowly the amplitude of the first harmonic decreases and higher harmonics (with increasing order) are generated. The decrease of the first harmonic is mainly due to the energy transfer to the other harmonics and only slightly due to the damping factor. With distances longer than shown in the figure above, also the higher harmonics (their absolute value) decrease again, due to energy transfer to even higher harmonics and due to the damping (the damping increases quadraticly with the order of the harmonic). Without the damping, the differential equation is unstable and the solution goes to $\pm\infty$.

In the Figure 5.3, the waveforms of a plane wave on a surface in terms of the horizontal and vertical components of the particle velocity is shown. The velocities are normalized with the initial amplitude of the fundamental harmonic component v_x. The initial waveform at $x/\bar{x} = 0$ is a sinusoid. In horizontal direction a shock profile

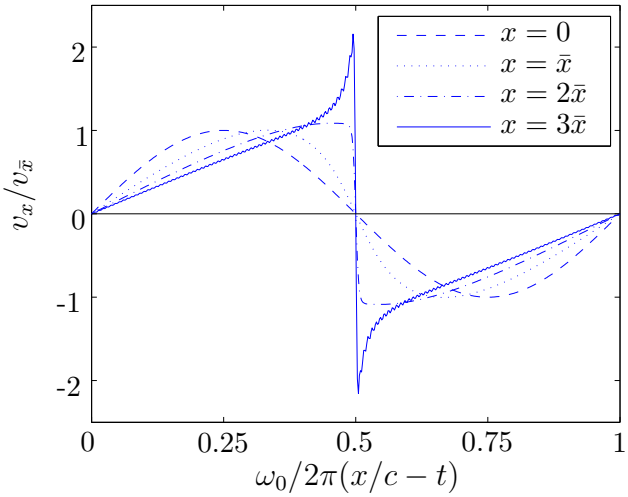

(a) Horizontal component (x-direction).

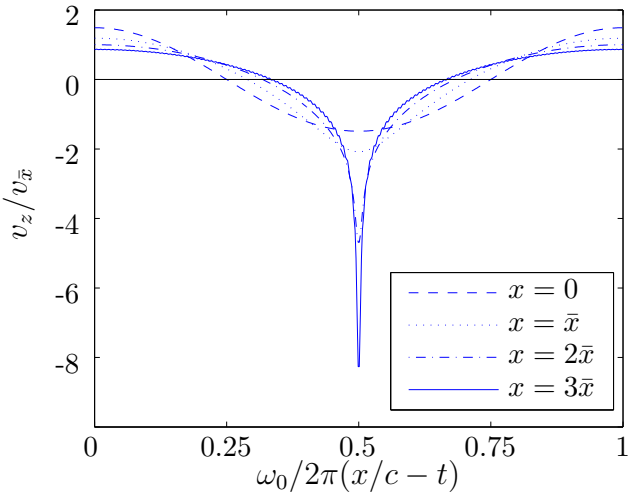

(b) Vertical component (z-direction).

Figure 5.3: Waveforms due to nonlinearity on the surface in terms of the horizontal and vertical components of the particle velocity.

is performed with increasing distance. The peak of the shock wave even exceeds the initial amplitude since the penetration depth of the harmonics decreases with their order, and the energy becomes more concentrated [33]. In the vertical direction a

pulse is formed whose polarity depends on the elastic constants. In steel, the pulse is negative.

Figure 5.3 coincides very well with the results in [33]. Just the the peak value in the horizontal component for $x = 3\bar{x}$ is different. One reason is that not all values necessary for the simulation were given in [33] and are therefore not the same. Another is that maybe different Runge-Kutta algorithms are used.

5.3 Nonlinear Parameter β_{R} for Rayleigh Waves

Based on the model presented in Section 5.2 a nonlinear parameter β_{R} similar to the β in the 1-d case with longitudinal waves (see Section 2.4) is derived and discussed.

5.3.1 Derivation of a Nonlinear Parameter β_R

First the dimensionless quantities

$$V_n = v_n/v_0\,, \quad \text{and} \quad X = x/\bar{x} \tag{5.40}$$

are introduced. With the dimensionless quantities, considering that $v_n^\star = v_{-n}$ and that v_n is real and without any damping ($\alpha_n = 0$), Equation (5.39) becomes

$$\frac{dV_n}{dX} = 2n^2 \sum_{m=n+1}^{N} R_{m,n-m} V_m V_{n-m} - n^2 \sum_{m=1}^{n-1} R_{m,n-m} V_m V_{n-m}\,. \tag{5.41}$$

Considering only three harmonics, Equation (5.41) can be written as

$$\frac{dV_1}{dX} = 2(R_{2,-1} V_2 V_1^\star + R_{3,-2} V_3 V_2^\star)\,, \tag{5.42}$$

$$\frac{dV_2}{dX} = 8R_{3,-1} V_3 V_1^\star - 4R_{1,1} V_1 V_1 \text{ and} \tag{5.43}$$

$$\frac{dV_3}{dX} = -9(R_{1,2} V_1 V_2 + R_{2,1} V_2 V_1)\,. \tag{5.44}$$

For relatively short distances $X << 1$ yields $V_1 >> V_2 >> V_3$ and $V_1 \approx 1 = \text{constant}$. This leads to the following approximations,

$$\frac{dV_1}{dX} \approx 0\,, \tag{5.45}$$

$$\frac{dV_2}{dX} \approx -4R_{1,1}V_1^2 \text{ and} \tag{5.46}$$

$$\frac{dV_3}{dX} \approx -9(R_{1,2}+R_{2,1})V_2V_1\,. \tag{5.47}$$

With consecutive integration the dimensionless harmonic velocity amplitudes become

$$V_1(X) = 1\,, \tag{5.48}$$

$$V_2(X) = -4R_{1,1}V_1^2X \text{ and} \tag{5.49}$$

$$V_3(X) = -18(R_{1,2}+R_{2,1})R_{1,1}V_1^3X\,. \tag{5.50}$$

Going back to the non-dimensionless harmonic velocity amplitudes yields

$$v_1(x) = v_0 = \text{const.}\,, \tag{5.51}$$

$$v_2(x) = -2\frac{\mu R_{1,1}}{\rho c_{\mathrm{R}}^3\zeta}k_0xv_1^2 \text{ and} \tag{5.52}$$

$$v_3(x) = \frac{9}{2}\frac{\mu^2(R_{1,2}+R_{2,1})R_{1,1}}{\rho^2c_{\mathrm{R}}^6\zeta^2}k_0^2x^2v_1^3\,. \tag{5.53}$$

Since the measurements are done for the velocity in z-direction at the surface, only the z-component of the velocity has to be considered following Equation (5.38). From Equation (5.17) it follows that $u_{z,n}$ at the surface is just a material dependent factor with $u_{z,n}(z=0) = (1+\eta\xi_l)$.

The nonlinear parameter β_{R} can be defined in terms of the velocity. However, in this case the β_{R} is not dimensionless but has the dimension $(\mathrm{m/s})^{-1}$. To stay consistent with the dimensionless definition of the β for the 1-d case with longitudinal waves (Section 2.4) the β_{R} for Rayleigh waves is defined in terms of the displacements.

Following Equations (5.38) and (5.19) the relation between the velocity amplitude in

z-direction of the nth harmonic, v_{zn}[1], and v_n is

$$v_{zn} = u_{z,n} v_n \,, \tag{5.54}$$

and the relation between the velocity and the displacement amplitude is given as

$$v_{zn}(x,z) = -i\omega n u_{zn}(x,z) \,. \tag{5.55}$$

This relation allows to define the dimensionless nonlinear parameter β_{R} for Rayleigh waves on the surface,

$$\beta_{\mathrm{R}} = \frac{u_{z2}}{k_0^2 x u_{z1}^2} = \frac{\mu R_{1,1}}{\rho c_{\mathrm{R}}^2 (1+\xi_l \eta)\zeta} \,. \tag{5.56}$$

The calculation of β_{R} in terms of the displacements is formally the same as in Equation (2.24). The formulation in terms of the material properties looks completely different from Equation (2.22). Especially since it contains the wave velocity c_{R} of the Rayleigh wave.

An additional nonlinear parameter β_{R3} can be defined by using the third harmonic displacement amplitude,

$$\beta_{\mathrm{R3}} = \frac{u_{z3}}{k_0^4 x^2 u_{z1}^3} = \frac{3}{2} \frac{\mu^2 (R_{1,2} + R_{2,1}) R_{1,1}}{\rho^2 c_{\mathrm{R}}^4 (1+\xi_l \eta)^2 \zeta^2} \,. \tag{5.57}$$

5.3.2 Justification and Verification of the Nonlinear Parameter β_R

In order to justify and verify the definition of the nonlinear parameter β_R results from the simulation as well as a laser ultrasound measurement of the second harmonic in Rayleigh waves by [10] are used. The simulation considers 128 harmonics and the values from Table 5.1 are used.

In Figure 5.4 the absolute value of the second harmonic velocity scaled by the first harmonic velocity over the propagation distance is shown. The upper Figure 5.4(a) shows the simulation for steel, the lower Figure 5.4(b) a measurement for a nickel base superalloy.

[1] v_{zn} includes both the negative and positive frequency part. The same yields for u_{zn}.

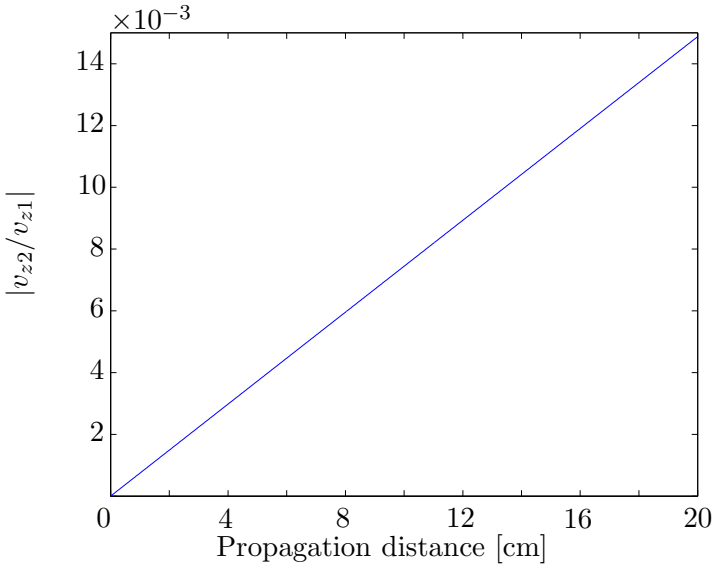

(a) Normalized second harmonic velocity amplitude in z-direction, model for steel (v_{z1}=constant).

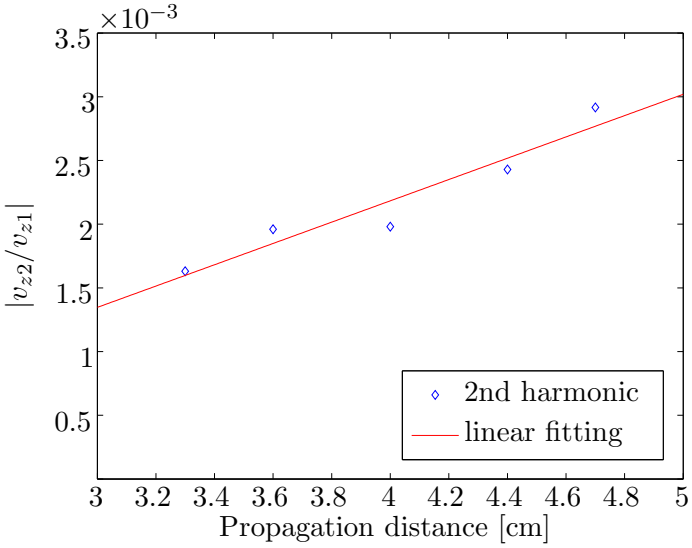

(b) Normalized second harmonic velocity amplitude in z-direction (v_{z1}=constant). Rayleigh wave measurement by Herrmann [10] for Nickel Base Superalloy.

Figure 5.4: Normalized second harmonic velocity amplitude in z-direction, out of model (steel) and measurement (Nickel Base Superalloy).

As described in Equation (5.52) the second harmonic in the approximation for calculating the β_{R} increases linearly with distance over the used short distance. This behavior is found in the simulation as well as in the measurement for short distances. For the first harmonic a constant value is observed.

For the third harmonic, the simulation for a short distance is given in Figure 5.5. As in the approximation for $v_{z3}(x)$ in Equation (5.53), the third harmonic is quadratic over the propagation distance. Note also that the normalized amplitude of the third harmonic is about forty times smaller than the second harmonic in Figure 5.4(a).

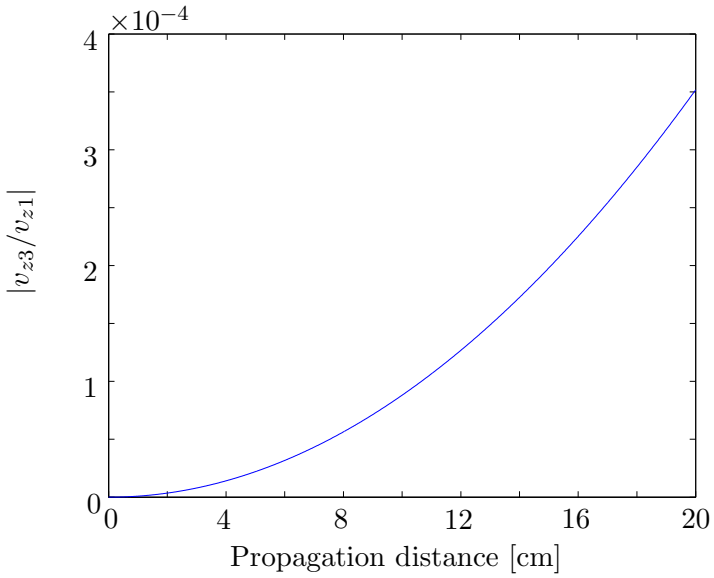

Figure 5.5: Normalized third harmonic velocity amplitude in z-direction (model with steel, v_{z1}=constant).

The next figure, Figure 5.6, deals with the dependency of the second harmonic velocity amplitude on the first harmonic velocity amplitude in z-direction. Shown is the result of the simulation in terms of the absolute values of the velocities where the second harmonic velocity amplitude is plotted over the first harmonic velocity amplitude squared for two different distances. The graph is a line whose slope increases with the distance. This behavior is in complete accordance with Equation (5.56) considering that the velocities are proportional to their displacements (Equation (5.55)) and that

β_{R} is a constant.

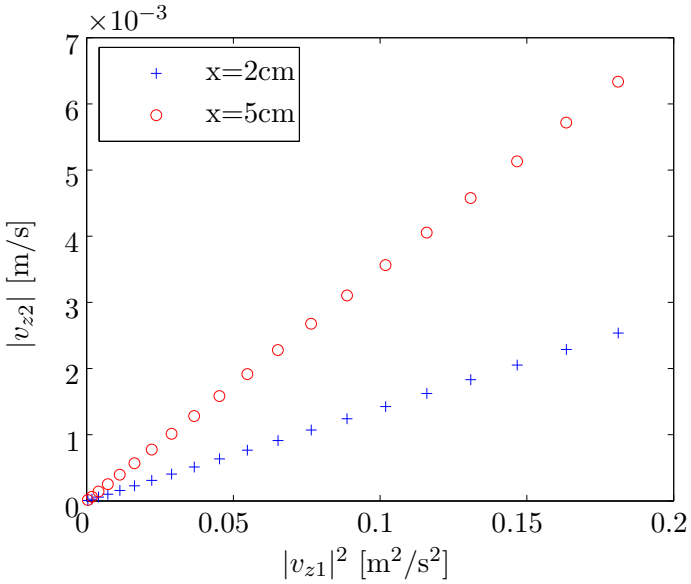

Figure 5.6: Second harmonic velocity amplitude over first harmonic velocity amplitude squared in z-direction (model with steel) at different propagation distances.

5.4 Further Discussions on the Nonlinear Parameter β_{R}

As seen in the previous section, there are a lot of similarities between the β for longitudinal waves in the 1-d case and the β_{R} defined for Rayleigh waves. This section discusses their properties, compares the two different β's and gives a physical explanation how they are connected.

5.4.1 Discussion and Comparison with β

Both nonlinear parameters, β and β_{R}, are only valid for not too long propagation distances. In [22] on page 49 this is shown for the 1-d case of longitudinal waves. A similar behavior of the harmonic amplitudes as partially shown in Figure 5.2 can be seen. However, for a practical use long distances do not occur anyway since other effects, e.g. scattering, play a more important role.

The next two figures deal with the connection between the nonlinearity parameter

β_R and the third order elastic constants A and B as well as between β and them. In Figure 5.7 β_R is plotted over A and B where A and B are given in percent of the original value given in Table5.1. The same yields for β in Figure 5.8.

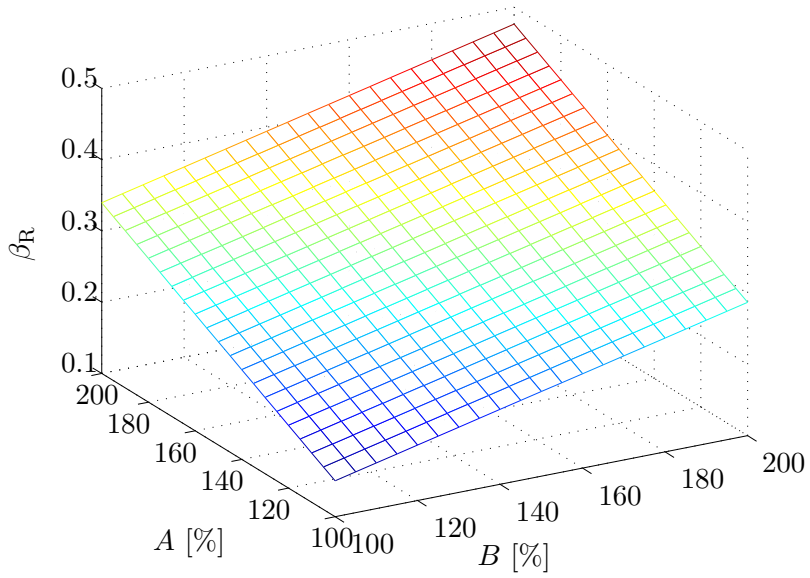

Figure 5.7: Nonlinear parameter β_R for Rayleigh waves dependent on the third order elastic constants A and B (A and B in percent of the values in Table 5.1).

Equation (5.56) shows a linear relation between β_R and $R_{1,1}$. Following Equations (5.22) to (5.36) $R_{m,l}$ is linear in the third order elastic constants. Consequently β_R is also linear in the third order elastic constants. The same yields for β following Equation (2.22). Therefore the plane in Figure 5.7 and 5.8 is completely flat.

Although, both, β and β_R are linear, they are not simply connected by a constant multiplier. The ratio between both is given in Figure 5.9. The plot has the form of a bent plane, therefore the linear dependencies of β and β_R on the third order elastic constants A and B are completely different. A similar behavior also exists for C, but it can hardly be seen since C with the values used (Table 5.1) is relatively small compared to A and B, and is therefore not shown.

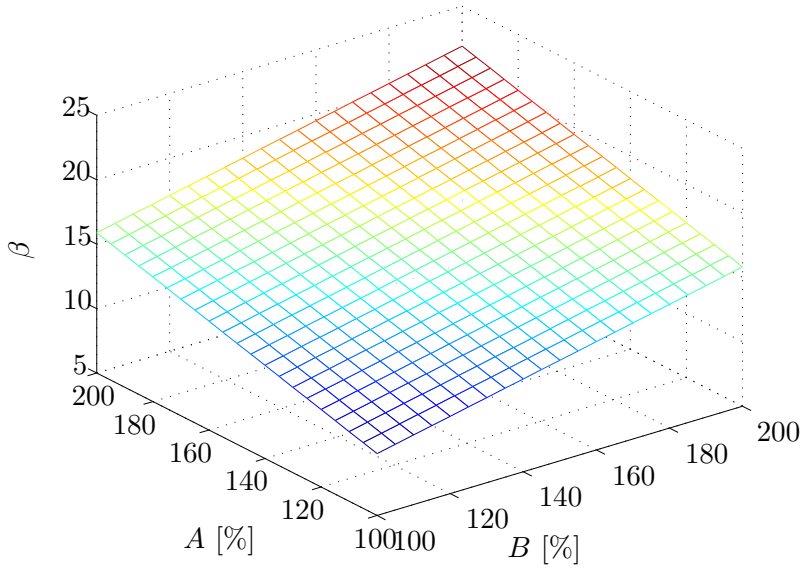

Figure 5.8: Nonlinear parameter β for longitudinal waves dependent on the third order elastic constants A and B (A and B in percent of the values in Table 5.1).

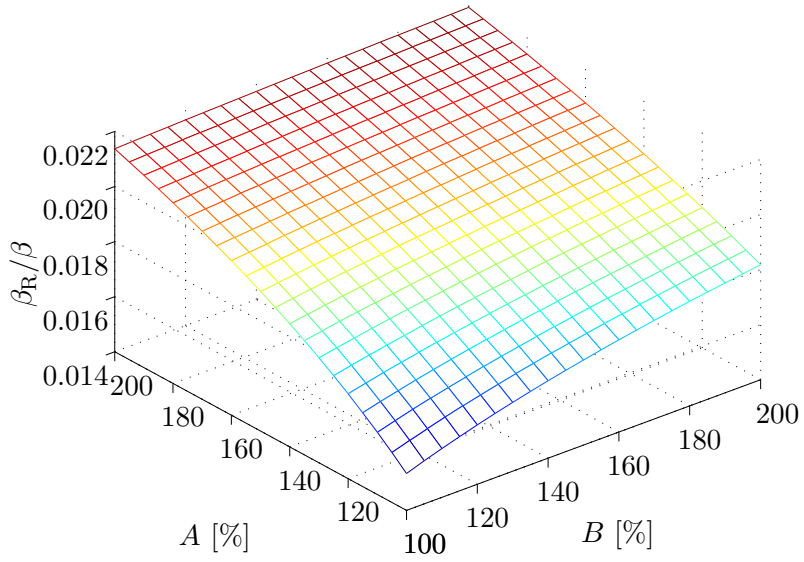

Figure 5.9: Ratio β/β_R dependent on the third order elastic constants A and B (A and B in percent of the values in Table 5.1).

A plot of the nonlinear parameter β_{R3} over the third order elastic constants is given in the Appendix C.1 where the quadratic relationship between β_{R3} and the third order elastic constants from Equation (5.56) can be seen.

5.4.2 Physical Connection between β and β_R

Shui and Solodov have made investigations on how second harmonics are generated by surface waves in nonlinear isotropic materials [25]. Based on a nonlinear reflection technique, they describe the generation of second harmonics by Rayleigh and Stoneley waves at the boundary or interface of isotropic solids. This is used to to obtain explicit analytical descriptions of Rayleigh and Stoneley wave nonlinear properties.

For this research, the most interesting part is how they describe the second harmonic generation physically. The principle that is used is shown in Figure 5.10. The left box

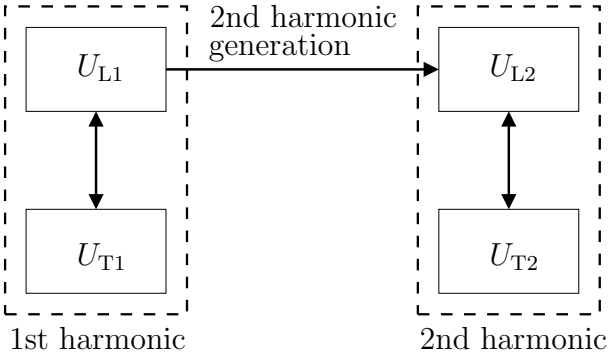

Figure 5.10: Second harmonic generation with Rayleigh waves according to [25].

represents the first harmonic, the right box the second harmonic. The first harmonic consist of a longitudinal and transverse/shear wave part. Only the longitudinal wave part generates higher harmonics, but due to the coupling of longitudinal and shear wave part at the surface of the body, the second harmonic also has a shear wave part.

This is supported by Equation (6.30) for a β for arbitrary crystal structure in [6],

$$\beta = -\frac{A_{ijklmn} N_j N_l N_n U_i U_k U_m}{A_{ijkl} N_j N_l U_i U_k}, \tag{5.58}$$

where A_{ijkl} and A_{ijklmn} are elastic constants, N_i are the column vectors of an orthogonal transformation matrix that transforms the coordinates such that one axis is parallel to the wave propagation direction, and U_i are the Cartesian coordinates of the unit particle displacement vector.

With the coordinates given in Figure 5.1 and a wave propagating in x-direction yields for a shear wave

$$\beta = -\frac{A_{ijklmn}\delta_{1j}\delta_{1l}\delta_{1n}\delta_{2i}\delta_{2k}\delta_{2m}}{A_{ijkl}\delta_{1j}\delta_{1l}\delta_{2i}\delta_{2k}} = 0\,. \tag{5.59}$$

Therefore shear/transverse waves cannot generate higher harmonics by themselves.

The mechanism shown in [25] supported by [6] explains the similarity between the β for longitudinal waves and the β_{R}.

5.4.3 A Different Definition for a Nonlinear Parameter for Rayleigh Waves

In [13] it is suggested to define a nonlinear parameter for Rayleigh waves as the ratio of the slope of the second harmonic to the first harmonic amplitude squared. The model used is also the one by [33]. Equation (5.46) is used to justify this nonlinear parameter and it is pointed out that this parameter can be determined without measuring absolute amplitudes. However, this is not true.

Equation (5.46) uses normalized quantities, e.g. V_1 is normalized such that it becomes 1. Therefore the absolute value of v_1 has to be known in order to determine the dimensionless nonlinear parameter, especially since V_1 is squared.

The only reason why this nonlinear parameter is dimensionless is the normalization and not a physical reason.

Another point is that values used for this nonlinear parameter appear only in the model and cannot be directly measured. Also requires the determination of a slope at least two measurements at different distances instead of one for the β_{R} defined in

this chapter.

5.5 Summary

To conclude this section the most important points are summarized. Based on the model in [33] a nonlinear parameter β_{R} is defined for Rayleigh waves. The definition is in accordance with the model as well as in accordance with measurements. β_{R} is linear in the third order elastic constants and is similar to the β for longitudinal waves due to the fact that the longitudinal part in Rayleigh waves is responsible for the higher harmonic generation. However, the connection between β and β_{R} in terms of the third order elastic constants is not just related by a constant multiplier since Rayleigh waves have always a shear/transverse wave part.

CHAPTER VI

THE NONLINEARITY PARAMETER AND FATIGUE DAMAGE

Some of the previous chapters deal with the dependency of the nonlinear parameter on elastic constants. In this chapter the connection between the nonlinear parameter, elastic constants and fatigue damage is discussed using a model suggested by Cantrell [7]. This is an important link for being able to make predictions about the expected remaining life of a specimen based on nonlinear measurements.

6.1 General Considerations

In the discussion of the nonlinearity parameter in the previous chapters, the dependency of β on the the third order elastic constants is emphasized since measurements have shown that in the course of the fatigue life of a specimen, the second order elastic constants remain approximately constant whereas higher order elastic constants change notably [14]. This characteristic of fatigue damage can therefore also be used for evaluating the validity of a model for fatigue damage.

A source of material nonlinearity in fatigued metals is dislocation motion. A dislocation is a linear crystallographic defect or irregularity within a crystal structure. It is assumed that two basic dislocation arrangements serve as building blocks for all dislocation substructures formed during fatigue of wavy slip metal. The first is the movement of dislocation monopoles under high stress and the related plastic deformation either by slip or climb. The second arrangement is a pair of monopoles forming a dipole that glides along a slip plane.

More details about dislocations can be found in [11, 15].

6.2 A Model for the Nonlinear Parameter Depending on the Fatigue Life

Cantrell has developed a model that describes how the nonlinear parameter depends on the fatigue life of a specimen that is fatigued by cyclic loading by considering dislocation motion in addition to the elastic nonlinear effects [7].

The assumptions are:

- fatigued metals possess internal (initial) stresses by the cyclic loading and
- a longitudinal stress perturbation applied to the initially stressed material gives rise to a longitudinal microstrain composed of an elastic strain contribution and two independent plastic strain contributions.

The total longitudinal strain ϵ,

$$\epsilon = \epsilon^e + \epsilon^{mp} + \epsilon^{dp} \tag{6.1}$$

consists of a longitudinal elastic strain component ϵ^e and two resolved longitudinal plastic strain components ϵ_{mp} due to the dislocation monopoles and ϵ_{dp} due to the dislocation dipoles.

In the next step, a stress-strain relationship for each component is derived and a series expansion is used to express each strain component as a series in the stress. Those series are summed up and the sum is used to determine a nonlinear parameter that includes contributions from all three sources of nonlinearity.

6.2.1 Contribution from Lattice Elasticity

Lattice elasticity yields the well-established relationship between stress and strain,

$$\sigma_{ij} = (\sigma_{ij})_{\mathbf{x}} + A^e_{ijkl}\epsilon^e_{kl} + \frac{1}{2}A^e_{ijklmn}\epsilon^e_{kl}\epsilon^e_{mn} + \dots \tag{6.2}$$

with initial stresses $(\sigma_{ij})_{\mathbf{x}}$ in the material at $\mathbf{x}$ and the Huang coefficients A^e_{ijkl} and A^e_{ijklmn}.

Considering a plane wave propagating along the x-axis in an isotropic material the nonlinearity parameter in this direction is expressed with the Huang coefficients,

$$\beta^e = -\frac{A^e_{111}}{A^e_{11}}\,, \tag{6.3}$$

where the Voigt notation is used.

Specializing to longitudinal stresses and strains in isotropic material and using Equation (6.2) the strain ϵ^e can be expressed in terms of the stress. In Equation (6.2) only the terms up to the second order are considered and the resulting quadratic equation is solved for ϵ^e. An expansion series [1] of the resulting equation leads together with $\sigma = \sigma_{11}$, $\epsilon^e = \epsilon_{11}$, $A^e_2 = A^e_{11}$ and $A^e_3 = A^e_{111}$ to

$$\epsilon^e = \frac{1}{A^e_2}\left(\sigma - \sigma_{\mathbf{x}}\right) - \frac{1}{2}\frac{A^e_3}{(A^e_2)^3}\left(\sigma - \sigma_{\mathbf{x}}\right)^2\,. \tag{6.4}$$

6.2.2 Contribution from Dislocation Monopoles

The contribution from dislocation monopoles is modeled by considering a relationship between the plastic shear strain and the resolved shear stress for dislocation motion. After some modifications, the strain with initial stress,

$$\epsilon^{mp} = \left(\frac{\partial \epsilon^{mp}}{\partial \sigma}\right)_{\mathbf{x}} \left(\sigma - \sigma_{\mathbf{x}}\right) + \frac{1}{2}\left(\frac{\partial^2 \epsilon^{mp}}{\partial \sigma^2}\right)_{\mathbf{x}} \left(\sigma - \sigma_{\mathbf{x}}\right)^2 + \dots\,, \tag{6.5}$$

is derived according to Cantrell. For the derivatives of the strain ϵ^{mp} with respect to the stress σ are the following approximations given,

$$\left(\frac{\partial \epsilon^{mp}}{\partial \sigma}\right)_{\mathbf{x}} \approx \frac{2}{3}\left(\frac{\Omega \Lambda^{mp} L^2 R}{G}\right) - \frac{16}{9}\left(\frac{\Omega \Lambda^{mp} L^2 R}{G}\right)^2 \bar{\sigma}_{\mathbf{x}} + \dots \quad \text{and} \tag{6.6}$$

$$\left(\frac{\partial^2 \epsilon^{mp}}{\partial \sigma^2}\right)_{\mathbf{x}} \approx \frac{24}{5}\left(\frac{\Omega \Lambda^{mp} L^4 R^3}{G^3 b^2}\right) \bar{\sigma}_{\mathbf{x}} + \dots\,, \tag{6.7}$$

where Ω is a conversion factor from shear strain to longitudinal strain, R the Schmid or resolving factor, Λ^{mp} the density of isolated dislocation monopoles, L the loop

[1] Used is the series $\sqrt{1+x} = 1 + \frac{1}{2}x - \frac{1}{8}x^2 + \dots$ for $|x| \leq 1$.

length, G the shear modulus, b the Burgers vector and $\bar{\sigma}_{\mathbf{x}}$ the initial longitudinal stress.

6.2.3 Contribution from Dislocation Dipoles

For the dislocation dipoles, Cantrell uses a force equation in between dislocations in the x-direction along their glide plane [11]. Cantrell considers only forces in the glide plane (x-direction) and neglects the force in the y-direction. Via a force equilibrium in the x-direction, and a Taylor series expansion of the following expression for $\bar{\sigma}^{dp}$ [2] is obtained,

$$\bar{\sigma} = \bar{A}_2^{dp}\bar{\epsilon}^{dp} + \frac{1}{2}\bar{A}_3^{dp}\left(\bar{\epsilon}^{dp}\right)^2 + \dots , \tag{6.8}$$

where

$$\bar{A}_2^{dp} = -\left(\frac{G}{4\pi\Omega R\Lambda^{dp}h^2(1-\nu)}\right) \quad \text{and} \tag{6.9}$$

$$\bar{A}_3^{dp} = \left(\frac{G}{4\pi\Omega^2 R(\Lambda^{dp})^2h^3(1-\nu)b}\right) . \tag{6.10}$$

Some of the variables used for the dipoles are the same with those for the monopoles. Additional variables are the equilibrium dipole height h, Poisson's ratio ν and the dipole density Λ^{dp}.

With respect to the initial stress configuration $\mathbf{x}$, the stress-strain relationship is written as

$$\sigma = \sigma_{\mathbf{x}} + A_2^{dp}\epsilon^{dp} + \frac{1}{2}A_3^{dp}(\epsilon^{dp})^2 + \dots . \tag{6.11}$$

Using the same procedure as in Section 6.2.1 delivers for the strain

$$\epsilon^{dp} = \frac{1}{A_2^{dp}}\left(\sigma - \sigma_{\mathbf{x}}\right) - \frac{1}{2}\frac{A_3^{dp}}{(A_2^{dp})^3}\left(\sigma - \sigma_{\mathbf{x}}\right)^2 + \dots . \tag{6.12}$$

[2] The bar indicates zero initial stress.

6.2.4 Material Nonlinearity in an Initially Stressed Solid with Dislocations

From Equation (6.1) together with Equations (6.4), (6.5) and (6.12) follows for the total strain

$$\epsilon = Q\left(\sigma - \sigma_{\mathbf{x}}\right) + R^{'}\left(\sigma - \sigma_{\mathbf{x}}\right)^2 + \dots\,, \tag{6.13}$$

where

$$Q = \frac{1}{A_2^e} + \frac{1}{A_2^{dp}} + \left(\frac{\partial \epsilon^{mp}}{\partial \sigma}\right)_{\mathbf{x}} \quad \text{and} \tag{6.14}$$

$$R = -\frac{1}{2}\left[\frac{A_3^e}{(A_2^e)^3} + \frac{A_3^{dp}}{(A_2^{dp})^3} - \left(\frac{\partial^2 \epsilon^{mp}}{\partial \sigma^2}\right)_{\mathbf{x}}\right]. \tag{6.15}$$

Keeping all terms up to the second order in Equation (6.13), solving for the stress σ and writing the result in terms of the expansion used in Section 6.2.1 leads to

$$\sigma = \sigma_{\mathbf{x}} + \frac{1}{Q}\epsilon - \frac{1}{2}\frac{2R^{'}}{Q^3}\epsilon^2 + \dots\,. \tag{6.16}$$

By comparing Equation (6.16) with Equation (6.2) the nonlinear parameter β including the dislocation motion is defined analog to Equation (6.3) as

$$\beta = -\frac{-2R^{'}/Q^3}{1/Q} = \frac{2R^{'}}{Q^2} = \frac{\beta^e + f^{mp}\beta^{mp} + f^{dp}\beta^{dp}}{\left(1 + f^{mp}\Gamma^{mp} + f^{dp}\Gamma^{dp}\right)^2}\,, \tag{6.17}$$

where the volume fractions f^{mp} and f^{dp} consider that monopoles and dipoles are not uniformly distributed over the material but rather in discrete fatigue-generated substructures. The different β's are nonlinearity parameters for each contribution with

$$\beta^e = -\frac{A_3^e}{A_2^e}\,, \quad \beta^{mp} = (A_2^e)^2\left(\tfrac{\partial^2 \epsilon^{mp}}{\partial \sigma^2}\right)_{\mathbf{x}} \text{ and } \quad \beta^{dp} = -(A_2^e)^2\frac{A_3^{dp}}{(A_2^{dp})^2}\,. \tag{6.18}$$

The gamma factors are,

$$\Gamma^{mp} = A_2^e\left(\frac{\partial \epsilon^{mp}}{\partial \sigma}\right)_{\mathbf{x}} \text{ and } \quad \Gamma^{dp} = \tfrac{A_2^e}{A_2^{dp}}\,, \tag{6.19}$$

respectively.

In a next step the model considers that the dislocation dipole contribution has a possible vein structure source and a possible PSB (permanent slip band) source depending on the state of fatigue. Thus it is written $f^{dp}\beta^{dp} = f_{vein}\beta^{dp}_{vein} + f_{BSBw}\beta^{dp}_{PSBw}$ and $f^{dp}\Gamma^{dp} = f_{vein}\Gamma^{dp}_{vein} + f_{PSBw}\Gamma^{dp}_{PSBw}$, where f_{vein} is the volume fraction of the vein structure and f_{PSBw} the volume fraction of the PSB wall structure that is about 10% of the PSB volume fraction f_{PSB}. A similar structure yields also for the dislocation monopole contribution, that has a vein structure source and a PSB source resulting from the generation of secondary dislocations. This is modeled as $f^{mp}\beta^{mp} = f_{vein}\beta^{mp}_{vein} + f_{BSB\sigma}\beta^{mp}_{PSB\sigma}$ and $f^{mp}\Gamma^{mp} = f_{vein}\Gamma^{mp}_{vein} + f_{PSB\sigma}\Gamma^{mp}_{PSB\sigma}$, where f_{vein} and $f_{PSB\sigma}$ are the volume fractions with $f_{PSB\sigma} = 0.1 f_{PSB}$.

The total β becomes finally

$$\beta = \frac{\beta^e + f_{vein}(\beta^{mp}_{vein} + \beta_v ein^{dp}) + 0.1 f_{PSB}(\beta^{mp}_{PSB\sigma} + \beta^{dp}_{PSBw}}{\left(1 + f_{vein}(\Gamma^{mp}_{vein} + \Gamma^{dp}_{vein}) + 0.1 f_{PSB}(\Gamma^{mp}_{PSB\sigma} + \Gamma^{dp}_{PSBw})\right)^2} . \tag{6.20}$$

6.3 Discussion

The change of β over the fatigue life as given in [7] looks reasonable. However, the biggest increase in β is in the first percent of the total life. This range is not of interest in determining the remaining life of a specimen. Yet there is still a measurable increase in the nonlinear parameter over the rest of the total life.

As mentioned earlier on, for the evaluation of the model the change of the second order elastic constants in the model has to be investigated. Therefore, starting from Equation (6.20), the second order elastic constant $\frac{1}{Q}$ in Equation (6.16) is calculated using the the Γ's, the β's and the volume fractions given in [7].

The second order elastic constant $\frac{1}{Q}$ is given as

$$\frac{1}{Q} = A_2^e \frac{1}{1 + f_v ein(\Gamma^{mp}_{vein} + \Gamma^{dp}_{vein}) + 0.1 f_{PSB}(\Gamma^{mp}_{PSB\sigma} + \Gamma^{dp}_{PSBw})} . \tag{6.21}$$

With the values in [7] at 100 percent of the total life, given in Table 6.1, there is a decrease in the second order elastic constant of about 49 % in the stress-controlled cyclic fatiguing and of about 44 % in the strain-controlled cyclic fatiguing compared to the elastic constant at the beginning of the life. In measurements the second order elastic constants stay almost constant. Note that the second order elastic constants determine the wave speed in the material.

Table 6.1: Values at 100 percent of the total life for stress- and strain-controlled fatiguing for nickel [7].

	stress-controlled	strain controlled
Γ_{vein}^{mp}	1.89	2.08
Γ_{vein}^{dp}	0.28	0.31
Γ_{PSBw}^{dp}	0.08	0.10
$\Gamma_{PSB\sigma}$	0.95	0.95
f_{vein}	0.35	0.4
f_{PSB}	0.158	0.217

The decrease in the second order elastic constants is also partially responsible for the increase of the modeled nonlinear parameter that is proportional to the ratio between the third order and second order elastic constant, as described in Equation (6.17). Therefore a decrease in the second order elastic constant of almost 50 % consequently doubles the nonlinear parameter.

A critical point in the model is determination of the dipole contribution. In the model a force equilibrium is only done in one direction, the glide plane. The force in the other direction is neglected although it probably also influences the motion.

A general problem of modeling the influence of dislocation motion is that values for the variables that are used are not easy to measure or determine. Some of them are also just estimated from other measurements.

Despite these obvious defects, the model by Cantrell is so far the only published model for the effect of fatigue damage on the nonlinear parameter and a first approach to this difficult problem. For further models it will be interesting to model not only the changes in one second and third order elastic constant, but in all elastic constants necessary to describe an isotropic material.

CHAPTER VII

CONCLUSION

This research demonstrates how signal processing issues influence the quality of nonlinear measurements. A windowing technique is developed to accurately calculate the amplitude of harmonics with special consideration of the characteristics of the harmonic signal, and the proposed scheme provides very accurate results. Moreover, a guarantee for the accuracy of the proposed windowing technique is provided.

A common problem of all techniques is the length of the available signal. The signal length is limited by the distance that the ultrasonic wave can propagate without any interferences by reflection and various other effects. Linear signal processing techniques cannot be applied to remove these interferences since the higher harmonics of the initial and reflected signal interact nonlinear due to the nonlinearity of the material. Also the naturally existing transient behavior of the ultrasonic signal at the beginning and the end reduces the viable range of a time signal.

A long signal with no changes in the amplitude, on the other hand, guarantees a precise determination of the harmonic amplitudes.

A further focus in this thesis is the definition of a nonlinear acoustic parameter for Rayleigh waves. This nonlinear parameter is developed using a model for Rayleigh waves in nonlinear isotropic materials. The physical connection to, and the similarity with, the nonlinear parameter for longitudinal waves is explained. Relative measurements of higher harmonic amplitudes in Rayleigh waves [10] show the behavior predicted for the nonlinear parameter developed. However, absolute measurements with different techniques still have to be done to prove the proposed nonlinear parameter for Rayleigh waves is correct.

Rayleigh waves are very promising for the detection of changes in the microstructure since fatigue theory [28] states that crack initiation takes place at or near the surface of a material where Rayleigh waves have concentrated all their energy.

For the prediction of the life of a sample, a model is needed that describes and links changes in the microstructure and the nonlinear acoustic parameter with the life. The only model [7] available at present is described and discussed. The model predicts a reasonable increase in the nonlinear parameter over life but also an undesirable increase in the second order elastic constants. However, the increase of the second order elastic constants is in contradiction to measurements where they stay almost constant. Therefore, a lot of work still has to be done in modeling the damage processes. Therefore, modeling the acoustic nonlinearity parameter of materials under fatigue load still remains to be an open problem.

APPENDIX A

NONLINEAR WAVE PROPAGATION

A.1 Approximation for the Solution of the Nonlinear Wave Equation

An approximation for the solution of the nonlinear wave Equation (2.21) can be obtained by using a perturbation method. The solution is also used for getting an expression for the nonlinear acoustic parameter β in terms of the first and second harmonic displacement amplitudes.

The nonlinear wave equation is given as

$$u_{,tt}(x,t) = c^2 u_{,xx}(x,t) - \beta c^2 u_{,xx}(x,t) u_{,x}(x,t)\,. \tag{A.1}$$

As an ansatz for an approximative solution

$$u(x,t) \approx u^{(0)}(x,t) + \beta u^{(1)}(x,t) \tag{A.2}$$

is chosen, where $u^{(0)}(x,t)$ is the solution for the linear wave equation ($\beta = 0$) and $u^{(1)}(x,t)$ considers the generation of a second harmonic by the first harmonic due to the nonlinearity.

Plugging the ansatz (A.2) in the nonlinear wave equation (A.1) yields

$$\begin{aligned} u^{(0)}_{,tt}(x,t) + \beta u^{(1)}_{,tt}(x,t) = c^2 \left(u^{(0)}_{,xx}(x,t) + \beta u^{(1)}_{,xx}(x,t)\right) \\ -\beta c^2 \left(u^{(0)}_{,xx}(x,t) + \beta u^{(1)}_{,xx}(x,t)\right)\left(u^{(0)}_{,x}(x,t) + \beta u^{(1)}_{,x}(x,t)\right)\,. \end{aligned} \tag{A.3}$$

Considering that $u^{(0)}(x,t) >> u^{(1)}(x,t)$ and that $u^{(0)}(x,t)$ is a solution for the linear wave equation reduces the equation above to

$$u^{(1)}_{,tt}(x,t) \approx c^2 u^{(1)}_{,xx}(x,t) - c^2 u^{(0)}_{,xx}(x,t) u^{(0)}_{,x}(x,t)\,. \tag{A.4}$$

A solution for the linear wave equation with the condition $u^{(0)}(x=0,t) = u_0 cos(\omega\tau)$, where $\tau = x/c - t$ is

$$u^{(0)}(x,t) = u_0 cos(\omega\tau)\,. \tag{A.5}$$

Equation (A.4) becomes then

$$u^{(1)}_{,tt}(x,t) \approx c^2 u^{(1)}_{,xx}(x,t) - \frac{1}{2}u_0^2 c^2 \left(\frac{\omega}{c}\right)^3 sin(2\omega\tau)\,. \tag{A.6}$$

With the ansatz $u^{(1)}(x,t) = xg(\tau)$ Equation (A.6) is used to determine $g(\tau)$,

$$\frac{1}{c}\frac{d}{d\tau}g(\tau) = -\frac{1}{4}u_0^2 \left(\frac{\omega}{c}\right)^3 sin(2\omega\tau)\,. \tag{A.7}$$

Integrating for τ results in

$$g(\tau) = -\frac{1}{8}u_0^2 \left(\frac{\omega}{c}\right)^2 cos(2\omega\tau) + (f \neq f(\tau))\,. \tag{A.8}$$

With the initial condition $u(x=0,t=0) = 0$ and $k = \omega/c$, the complete approximation solution for the nonlinear wave equation becomes

$$u(x,t) = \frac{1}{8}\beta u_0^2 k^2 x + u_0\, cos(kx - \omega t)) - \frac{1}{8}\beta u_0^2 k^2 x\, cos(2(kx - \omega t))\,, \tag{A.9}$$

as shown in Equation (2.23).

APPENDIX B

SIGNAL PROCESSING FOR NONLINEAR MEASUREMENTS

B.1 Commonly used Windows

- Bartlett (triangular) window

$$w[n] = \begin{cases} \frac{2n}{M-1}, & 0 \leq n \leq (M-1)/2, \\ 2 - \frac{2n}{M-1}, & (M-1)/2 < n \leq M-1, \\ 0, & \text{otherwise} \end{cases}$$

- Hanning window

$$w[n] = \begin{cases} 0.5 - 0.5\cos(\frac{2\pi n}{M-1}), & 0 \leq n \leq M-1, \\ 0, & \text{otherwise} \end{cases}$$

- Hamming window

$$w[n] = \begin{cases} 0.54 - 0.46\cos(\frac{2\pi n}{M-1}), & 0 \leq n \leq M-1, \\ 0, & \text{otherwise} \end{cases}$$

- Blackman window

$$w[n] = \begin{cases} 0.42 - 0.5cos(\frac{2\pi n}{M-1}) + 0.08cos(\frac{4\pi n}{M-1}), & 0 \leq n \leq M-1, \\ 0, & \text{otherwise} \end{cases}$$

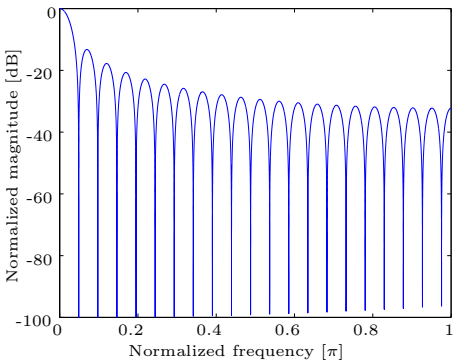

(a) Rectangular window (length 41).

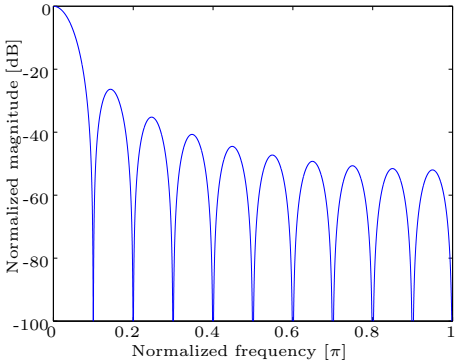

(b) Bartlett window (length 41).

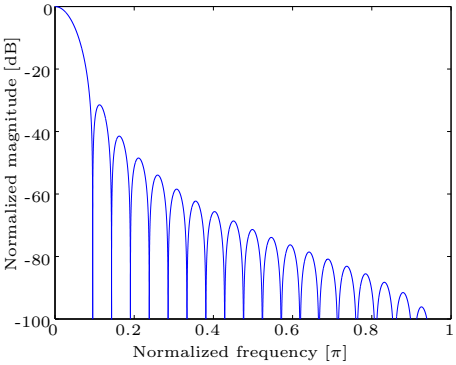

(c) Hanning window (length 41).

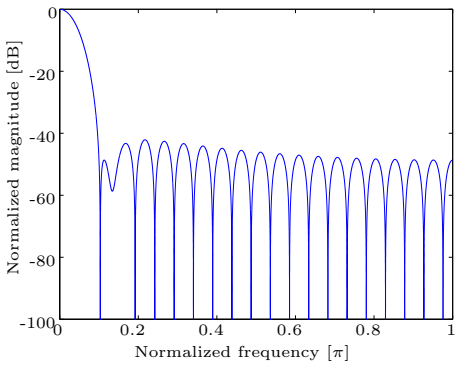

(d) Hamming window (length 41).

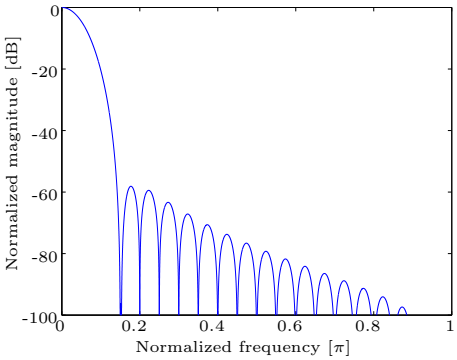

(e) Blackman window (length 41).

Figure B.1: Commonly used windows (frequency domain, length 41).

B.2 STFT in Terms of Signal and Window Spectra

From the Fourier transform theory it is known that the Fourier transform of the product of two sequences is given by the convolution of their respective Fourier transform [20],

$$x(t)w(t) \overset{\mathcal{F}}{\leftrightarrow} \frac{1}{2\pi} \int_{-\infty}^{\infty} X(e^{j\Theta}) W(e^{j(\omega-\Theta)}) d\Theta \,. \tag{B.1}$$

If $w(t)$ is additionally delayed by the time u we receive

$$x(t)w(t-u) \overset{\mathcal{F}}{\leftrightarrow} \frac{1}{2\pi} \int_{-\infty}^{\infty} X(e^{j\Theta}) e^{-j(\omega-\Theta)u} W(e^{j(\omega-\Theta)}) d\Theta \,. \tag{B.2}$$

Therefore the STFT may also be expressed in terms of signal and window spectra

$$F_x(t,\nu;h) = \frac{1}{2\pi} \int_{-\infty}^{\infty} X(\xi) W(\xi-\nu) e^{j2\pi(\xi-\nu)t} d\xi \tag{B.3}$$

where X and W are respectively the Fourier transforms of x and w [19].

APPENDIX C

RAYLEIGH WAVES FOR NONLINEAR MEASUREMENTS

C.1 Nonlinear Parameter β_{R3}

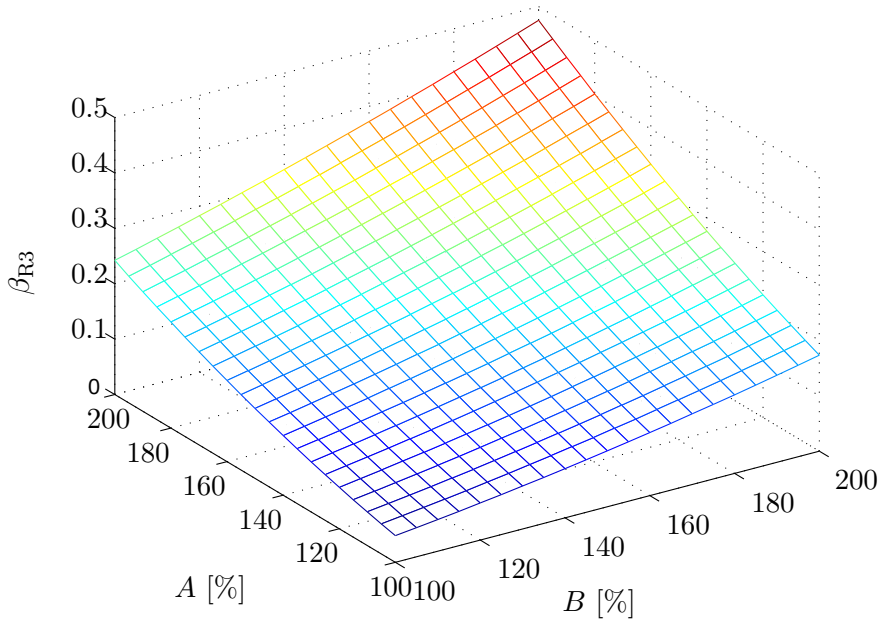

Figure C.1: Nonlinear parameter β_{R3} for Rayleigh waves dependent on the third order elastic constants A and B (A and B in percent of the values in Table 5.1).

REFERENCES

[1] Achenbach, J., *Wave Propagation in Elastic Solids*. Amsterdam: Elsevier, 1st ed., 1999.

[2] Al'i, G., Hunter, J., and Parker, D., "Hamiltonian Equations for Scale-invariant Waves," in *Studies in Applied Mathematics*, vol. 108, pp. 305–321, 2002.

[3] Bendat, J. S. and Piersol, A. G., *Random Data: Analysis and Measurement Procedures*. New York: Wiley, 2nd, rev. and expanded ed., 1986.

[4] Bronstein, I. N., Semendjaev, K. A., and Musiol, G.and Muhlig, H., *Taschenbuch der Mathematik*. Thun and Frankfurt am Main: Verlag Harri Deutsch, 5th ed., 2001.

[5] Cantrell, J. H., "Acoustic-radiation Stress in Solids I," in *Theory. Phys. Rev.*, vol. B 30, pp. 3214–3220, 1984.

[6] Cantrell, J. H., "Fundamentals and Applications of Nonlinear Ultrasonic Nondestructive Evaluation," in *Ultrasonic Nondestructive Evaluation* (Kundu, T., ed.), part 6, pp. 363–434, Boca Raton, Florida: CRC Press, 2004.

[7] Cantrell, J. H., "Substructural Organization, Dislocation Plasticity and Harmonic Generation in Cyclically Stressed Wavy Slip Metals," in *Proceedings of The Royal Society London A*, vol. 460, pp. 757–780, 2004.

[8] Hamilton, M. F. and Blackstock, D. T., *Nonlinear Acoustics*. London: Academic Press, 1997.

[9] Harris, F. J., "On the Use of Windows for Harmonic Analysis with the Discrete Fourier Transform," in *Proceedings of the IEEE*, vol. 66 (1), January 1978.

[10] Herrmann, J., *Generation and Detection of Higher Harmonics in Rayleigh Waves Using Laser Ultrasound*. Master thesis, School of Civil and Environmental Engineering, Georgia Institute of Technology, August 2005.

[11] Hull, D. and Bacon, D., *Introduction to Dislocations*. Butterworth-Heinemann, 4 ed., 2001.

[12] Hurlebaus, S., *Laser Generation and Detection Techniques for Developing Transfer Functions to Characterize the Effect of Geometry on Elastic Wave Propagation*. Master thesis, School of Civil and Environmental Engineering, Georgia Institute of Technology, September 1996.

[13] Hurley, D. H. and Telschow, K. L., "Probing Acoustic Nonlinearity by Mixing Surface Acoustic Waves," in *Review of Progress in Quantitative Nondestructive Evaluation*, vol. 20B, pp. 1236–1241, 2001.

[14] Kim, J.-Y. Private conversation; Woodruff School of Mechanical Engineering, Georgia Institute of Technology.

[15] Kov'acs, I. and Zsoldos, L., *Dislocations and Plastic Deformation*. Pergamon Press, 1973.

[16] Krishnan, S. and O'Donnell, M., "Transmit Aperture Processing for Nonlinear Contrast Agent Imaging," in *Ultrasonci Imaging*, vol. 18-2, pp. 77–105, 1996.

[17] Landau, L. and Lifshitz, E., *Theory of Elasticity*. Massachusetts: Addison-Wesley, Reading, 1959.

[18] Landau, L. and Lifshitz, E., *Theory of Elasticity*. New York: Pergamon, 2nd ed., 1981.

[19] Lim, J. S. and Oppenheim, A. V., *Advanced Topics in Signal Processing*. Englewood Cliffs, New Jersey 07632: Prentice Hall, 1988.

[20] Mallat, S., *A Wavelet Tour of Signal Processing*. Academic Press, 2nd ed., 1999.

[21] Meyendorf, N. G., Nagy, P. B., and Rokhlin, S. I., *Nondestructive Materials Characterization: With Applications to Aerospace Materials*. Berlin; New York: Springer, 2004.

[22] Naugolnykh, K. and Ostrovsky, L., *Nonlinear Wave Processes in Acoustics*. Cambridge University Press, 1998.

[23] Ohara, Y., Kawashima, K., Yamada, R., and Horio, H., "Evaluation of Amorphous Diffusion Bonding by Nonlinear Ultrasonic Method," in *Review of Quantitative Nondestructive Evaluation*, vol. 23, pp. 944–951, 2004.

[24] Oppenheim, A. V. and Schafer, R. W., *Discrete-Time Singal Processing*. Upper Saddle River, New Jersey 07458: Prentice Hall, 2nd ed., 1998.

[25] Shui, Y. and Solodov, I. Y., "Nonlinear Properties of Rayleigh and Stoneley Waves in Solids," in *Journal of Applied Physics*, vol. 64(11), pp. 6155–6165, 1988.

[26] Shull, D., Hamilton, M., Ll'insky, Y., and Zabolotskaya, E., "Harmonic Generation in Plane and Cylindrical Nonlinear Rayleigh Waves," in *J. Acoust. Soc. Am.*, vol. 94 (1), July 1993.

[27] Smith, J. O., *Mathematics of the Discrete Fourier Transform (DFT)*. http://www.w3k.org/books/: W3K Publishing, 2003.

[28] Suresh, S., *Fatigue of Materials*. New York: Cambridge University Press, 2nd ed., 1998.

[29] Thornburg, D. H. and Leistikow, R. J., "An Iterative Filterbank Approach for Extracting Sinusoidal Parameters from Quasiharmonic Sounds," in *Proceedings of 2003 IEEE Workshop on Applications of Signal Processing to Audio and Acoustics*, (New Paltz, New York), IEEE, 2003.

[30] Truell, R., Elbaum, C., and B., C. B., *Ultrasonic Methods in Solid State Physics*. Academic Press, 1969.

[31] Viktorov, I., *Rayleigh and Lamb Waves, Physical Theory and Applications*. Plenum Press New York, 1st ed., 1967.

[32] Wilkinson, J., *Rounding Errors in Algebraic Processes*. Prentice-Hall, 1963.

[33] Zabolotskaya, E., "Nonlinear Propagation of Plane and Circular Rayleigh Waves in Isotropic Solids," in *J. Acoust. Soc. Am.*, vol. 91 (5), May 1992.